Histone lactylation: a new epigenetic mark in the malaria parasite *Plasmodium*

Ibtissam Jabre[1a] & Nana Efua Andoh[1a], Juliana Naldoni[1], William Gregory[1], Haddijatou Mbye[1], Chae Eun Yoon[2,3], Aubrey J. Cunnington[2,3], Athina Georgiadou[2,3], Andrew M. Blagborough[1], Catherine J. Merrick[1*]

[1] Department of Pathology, University of Cambridge, Tennis Court Road, Cambridge, CB2 1QP, UK.

[2] Section of Paediatric Infectious Disease, Department of Infectious Disease, Imperial College London, London, United Kingdom.

[3] Centre for Paediatrics and Child Health, Imperial College London, London, United Kingdom.

[a] Equal contributions

* To whom correspondence should be addressed:
Department of Pathology, Cambridge University, Tennis Court Road, Cambridge, CB2 1QP, UK
Tel: (+44) 1223 333330
CJM: Email: cjm48@cam.ac.uk

ABSTRACT

Epigenetic processes play important roles in the biology of the malaria parasite *Plasmodium falciparum*. Here, we characterised a new epigenetic mark, histone lactylation, recently discovered in humans: it was found in two human malaria parasites, *P. falciparum* and *P. knowlesi*, and also *in vivo* in two rodent malaria models. Histones were lactylated rapidly in response to elevated lactate levels, and rapidly delactylated when lactate levels fell. Thus, this mark is well-placed to act as a metabolic sensor, since severe falciparum malaria characteristically leads to hyperlactataemia. Mass spectrometry showed that lysines on several parasite histones could be lactylated, as well as many non-histone chromatin proteins. Histone lactylation was less abundant and less inducible in *P. knowlesi* than *P. falciparum*, suggesting that *P. falciparum* may have evolved particular epigenetic responses to this characteristic feature of its pathology. Finally, in the rodent model *P. yoelii*, hyperlactataemia correlated with parasite transcriptomic programmes that suggested metabolic 'dormancy'.

KEYWORDS: Malaria, *Plasmodium*, epigenetics, histone lactylation, lactyl lysine

INTRODUCTION

Human malaria occurs when protozoan *Plasmodium* parasites infect red blood cells. Six *Plasmodium* species can cause malaria in humans, including the main agent of severe and fatal malaria, *P. falciparum*, and the zoonotic macaque parasite *P. knowlesi.* These two are currently the only human malaria parasites that can be cultured continuously *in vitro.*

Clinical malaria has many characteristic pathological features, one of which is hyperlactataemia. This is clinically defined as a level of blood lactate above 5mM, but patients with falciparum malaria can reach at least 15mM [1,2]. Parasites in the bloodstream respire by glycolysis, producing lactate, and they also cause their host erythrocytes to adhere to capillary walls, impeding blood flow and promoting anaerobic respiration in host tissues. Collectively, this results in hyperlactataemia, which is predictive of severe disease and death, as it can lead to the fatal malaria syndrome of metabolic acidosis and respiratory distress [3].

Plasmodium parasites could benefit from being able to sense the metabolic environment in their host and modify virulence accordingly – for example, by increasing commitment to sexual stages that are competent for transmission to new hosts, or by modulating cytoadherence of infected erythrocytes. This fascinating area of host-parasite biology is increasingly being explored, with aspects of blood chemistry including levels of glucose, magnesium and S-adenosylmethionine being proposed to influence the virulence of *P. falciparum* parasites [4-7].

Blood lactate has yet to be fully explored in this context, but since it correlates with parasite load and disease severity, it could potentially serve as both a 'quorum sensor' and a measure of host stress. In one human infection study, lactate was linked to the expression pattern of a key virulence gene family, *var*, which encodes variant adhesins expressed on infected erythrocytes [1]. The *var* gene family is known to be epigenetically controlled by histone acetylation and methylation. Epigenetics also plays other prominent roles in *Plasmodium* biology, controlling aspects of virulence including alternate invasion pathways and sexual stage commitment (gametocytogenesis) [8]. In a recent *in vitro* study, gametocytogenesis was also linked to lactate, with parasites cultured in added lactate converting to gametocytes at an elevated rate [9].

Here, we explored lactate as a potential epigenetic modifier in *Plasmodium*, following the recent discovery of lactyl-lysine as a new epigenetic mark in mammalian cells, similar to the well-characterised acetyl-lysine [10]. Since its discovery in 2019, this epigenetic mark has been heavily explored in the context of human cells in high-lactate environments – primarily tumours experiencing the Warburg effect [11,12]. It has not yet been explored in the context of malaria, a disease characterised by systemic hyperlactataemia; however, we did recently observe that histone lactylation could occur in *P. falciparum*, and hence proposed this as a new virulence modifier in *Plasmodium* [13]. We now report that the epigenetic mark is conserved in several *Plasmodium* species, occurring both *in vitro* and *in vivo*. It appears on many histone lysine residues, is rapidly labile and is responsive to lactate levels both in culture and in mammalian host blood. Therefore, it could have many virulence-modulating roles.

76

77 **RESULTS**

78 *Plasmodium* histones are inducibly lactylated

79 We first measured the level of lactyl-lysine in *Plasmodium* histones after treating cultured
80 parasites with increasing levels of lactate. Trophozoite-stage *P. falciparum* parasites were
81 exposed to 5-25mM lactate, added to the culture media for 12h. **Figure 1A** shows that their
82 histones were inducibly and titratably lactylated, with histone H4 showing the strongest
83 lactyl-lysine signal. An antibody identifying a single lactylated residue on histone H4 (K12)
84 confirmed that the general lactyl-lysine antibody recognised this histone, but lactylation of
85 the K12 residue was not strongly inducible **(fig 1B)**. We conducted the same experiments on
86 a second species, *P. knowlesi*, and showed that histone lactylation was similarly inducible
87 **(fig 1C)**. It was, however, much less abundant than in *P. falciparum*, since greater amounts
88 of parasite extract were required to detect similar signals on *P. knowlesi* histones, and the
89 specific residue H4K12La was barely detectable **(fig 1D)**.
90 We then investigated whether this phenomenon occurs naturally *in vivo* during
91 malaria. The rodent model species *P. yoelii*, strain 17XL, can generate severe
92 hyperlactataemia [14], and blood lactate levels in mice infected with *P. yoelii* 17XL did indeed
93 correlate with histone lactylation in the parasite **(fig 1E)**. Notably, not all rodent malaria
94 models lead consistently to hyperlactataemia and in the *P. berghei* ANKA strain, which does
95 not [14], we did not observe a strong correlation between blood lactate and histone
96 lactylation **(fig S1)**. Overall, these results revealed that there is a conserved pathway for
97 histone lactylation in *Plasmodium,* induced by hyperlactataemia.

98 Histone lactylation is rapidly inducible and reversible

99 We next investigated the time dynamics of the modification: **figure 1** shows that it can occur
100 within 12h and 8h in *P. falciparum* and *P. knowlesi* respectively, but it does not show how
101 fast the modification was actually added, or how fast it would be removed if exogenous
102 lactate levels subsequently fell. To investigate this, parasites were tightly synchronised at
103 rings, washed into fresh media, exposed to a pulse of 25mM lactate when they reached
104 early trophozoites, then followed by western blotting at intervals over the subsequent 20-
105 24h. (25mM lactate, for 12h in *P. falciparum* or 8h in *P knowlesi* due to its shorter cell cycle,
106 was chosen for these and subsequent experiments because, from **figure 1**, this induced the
107 strongest histone lactylation, without markedly affecting parasite growth **(fig S2)**, whereas
108 even higher levels of ≥ 30mM over 48h were previously reported to affect parasite growth
109 in *P. falciparum*[15]).
110 **Figure 2A** shows that histone lactylation rose within just 2h of exposure; continued
111 to rise after 6h, and then fell back slightly after 12h. This was surprising, but we surmised
112 that it may be because of a natural cell-cycle-related pattern in histone lactylation, since
113 parasite metabolism, which peaks in trophozoites, produces its own endogenous lactate.
114 This was confirmed by an identical parallel timecourse in which no exogenous lactate was

115 added **(fig 2A**: grey bars**)**. Here, histone lactylation was still induced, but to a much lesser
116 extent, peaking in the mid-trophozoite stage (~30-32hpi) and falling back slightly in late
117 trophozoites (~36-38hpi).
118 To measure the dynamics of de-lactylation, parasite cultures were washed after 12h
119 and then followed at subsequent timepoints 6 and 12h later (re-washing at each of these
120 points to keep the lactate levels in the media low). By 6h (i.e. in schizonts at ~42-44hpi), the
121 level of histone lactylation had reverted to baseline levels. Again, this followed the 'natural'
122 cell cycle pattern, which was greatly amplified by exposure to exogenous lactate. Thus,
123 histone lactylation was rapidly responsive – in both directions – to changes in the lactate
124 content of the media.
125 We repeated these experiments in *P. knowlesi* **(fig 2B)**: again, the histone lactylation
126 signal was inducible across the trophozoite stage of the cell cycle, while background levels
127 of lactylated histones were low, variable, and not clearly cell-cycle-regulated in this species
128 **(fig 2B**: grey bars**)**. As in **figure 1**, the signal was weaker than in *P. falciparum:* 4-5 times the
129 quantity of *P. knowlesi* histones was required to detect comparable levels of histone
130 lactylation by western blotting.
131 To measure the extent of endogenous lactate production in our parasite culture
132 system, we measured lactate levels in the media, both when parasites were cultured under
133 standard conditions (reducing the parasitaemia and changing the media every 48h), and also
134 when they were allowed to grow continuously to the point of 'crashing' (the term for
135 parasite death due to high parasitaemia and exposure to spent media [16]) **(fig 2C,D)**. As
136 expected, media lactate levels correlated with parasitaemia, reaching only ~5mM within 2
137 days as a culture of *P. falciparum* grew from 0.5% to 4.6% parasitaemia **(fig 2C)**. When the
138 culture was allowed to 'crash', lactate levels peaked at ~10mM **(fig 2C)**. The profile of
139 lactate production was similar in *P. knowlesi* cultures, although this parasite is more
140 resistant than *P. falciparum* to 'crashing', so these parasites could grow exponentially for at
141 least 3 days, producing lactate continuously and reaching 11.5mM by day-4 **(fig 2D)**. We
142 also followed histone lactylation in *P. falciparum* over 72h by western blotting, confirming
143 that it fluctuated in a stage-dependent manner even as lactate accumulated in the media,
144 with lactylation being consistently higher in trophozoites and lower in rings **(fig 2E).**
145 Overall, these data show that routine culture of both parasite species can expose them
146 to significant but modest lactate fluctuations. Routine cultures can reach the clinical
147 threshold for hyperlactataemia (5mM), which is sufficient to induce some histone lactylation
148 **(fig 1)**, but is much lower than the levels attained in human patients with severe malaria [1,2].

149 <u>Histone acetylation is affected by exposure to high lactate</u>

150 In human cells, both acetylation and lactylation have been detected on the same histone
151 lysine residues, and it has been suggested that histone acetyltransferase enzymes may
152 moonlight as lactylases [10]. This raised the possibility that in *Plasmodium*, histone lactylation
153 could reciprocally affect histone acetylation – a well-established factor in gene expression
154 regulation.

155 We tested this by western-blotting for acetyl H4 and acetyl H3 under conditions of
156 high lactate exposure, as in **figure 1. Figure 3A-D** shows a trend towards lactate-inducible
157 acetylation, with acetylation of H3 rising up to 2-fold after exposure to 25mM lactate and
158 acetylation of H4 rising an average of 2-fold, albeit with less consistency between
159 experiments. Thus, acetylation was less strongly lactate-inducible than lactylation, but the
160 two histone marks could be mutually regulated by lactate.
161 We also followed the time dynamics of histone acetylation following lactate exposure,
162 using timecourses as in **figure 2 (fig 3E-H).** Acetylation did not vary greatly across the
163 normal cell cycle (fluctuations were less than 2-fold) but after exposure to 25mM lactate,
164 histones were, again, additionally acetylated, particular on H4 in *P. falciparum*. This occured
165 as rapidly as lactylation – within 2h – but deacetylation was not equally rapid after lactate
166 removal (this was also seen particularly on H4 in *P. falciparum* **(fig 3F)**). This may suggest
167 that histone acetyltransferase activity is shared for both modifications, whereas deacetylase
168 activity is not.
169
170 <u>Histone lactylation is distributed throughout the nucleus</u>

171 In *P. falciparum,* certain histone modications are specifically associated with
172 heterochromatin, which tends to be located at the nuclear periphery, marked by
173 heterochromatin protein 1 (HPI) [17], whereas other modifications associated with
174 euchromatin appear throughout the nucleoplasm. We investigated the location of histone
175 lactylation using immunofluorescence microscopy **(fig 4)**. We found no evidence for
176 compartmentalisation of lactylated histones, with both the general lactyl-lysine signal **(fig**
177 **4A)** and the specific signal for H4K12 **(fig 4B)** appearing throughout the nuclei of all parasite
178 stages. Neither signal colocalised with HP1, and both appeared similar to the pan-nuclear
179 distribution of histone acetylation (**fig S3**). The great majority of lactyl-lysine signal was
180 nuclear **(fig 4A)**, suggesting that there is little lactylated protein in the cytoplasm of
181 *Plasmodium.*

182 <u>Histone lactylation occurs on multiple histone lysine residues</u>

183 For a comprehensive view of the histone lysine residues that can be lactylated in both *P.*
184 *falciparum* and *P. knowlesi*, we used liquid chromatography-tandem mass spectrometry (LC-
185 MS/MS). Trophozoite-stage parasites were either exposed or not exposed to 25mM lactate
186 and their histones were acid-extracted from chromatin in biological triplicate. In a single
187 pilot experiment, histones were also extracted from mixed stage cultures (+/- 25mM
188 lactate), enabling detection of KLa sites in all stages of the asexual cycle. Histone integrity
189 and the induction of lactylation were confirmed via Coomassie-stained SDS-PAGE and by
190 immunoblotting for KLa **(Fig S4)**.
191 Mass spectrometry on the histone-containing region of the gel identified all eight
192 histones (H2A, H2A.Z, H2B, H2B.Z, H3, H3.3, CenH3 and H4), with sequence coverage
193 >67.5% except in the case of CenH3 **(Tables S1-4).** We then mapped KLa sites, as previously

194 reported [10] **(Fig S5A)**, revealing 16 and 21 KLa sites in *P. falciparum* and *P. knowlesi*
195 respectively **(Fig 5A)**. These were unevenly distributed across the histone tails and almost
196 all KLa sites could also be acetylated **(Fig S5B, Tables S1-4).** Interestingly, despite the
197 histone sequences being highly conserved between *Plasmodium* species, the majority of KLa
198 sites were species-specific, suggesting that this modification may have species-specific
199 function(s). As expected from **figures 1-2**, lactylation of some residues was induced after
200 exposure to 25mM lactate, but inducibility varied between residues and also between
201 species **(fig 5B).** It also varied in trophozoites versus mixed-stage cultures, implying that
202 some residues may be lactylated stage-specifically.

203 Cross-talk may occur between histone lactylation, acetylation and methylation

204 Acetylation and lactylation were often detected on the same lysine residues, both in our
205 data and previously in human cells [10]. Therefore we sought to investigate whether lactate
206 exposure in the trophozoite stage could induce changes in the distribution of histone
207 acetylation (Kac), as well as di- and tri- methylation (K(me2), K(me3)).
208 There was no dramatic change in the distribution of Kac sites after exposure to
209 25mM lactate, and Kac remained the most abundant histone modification, as previously
210 reported [18] **(Tables S1-4)**. Almost all KLa sites were also detected as Kac but the converse
211 was not true: ~65% of Kac sites were unique **(Fig S5B)**. After lactate exposure, 44% of
212 histone KLa sites in *P. falciparum* and 17% of those in *P. knowlesi* were significantly induced
213 (P-value ≤ 0.05) **(fig 6A, top panel; Tables S1-2)**, corroborating the observation from **figures**
214 **1-2** that lactylation was more strongly inducible in *P. falciparum* than in *P. knowlesi.* By
215 contrast, only ~12% and ~7% of histone Kac sites, respectively, were significantly up- or
216 down-regulated. Hence, relatively few Kac sites (amongst many that can be acetylated)
217 must be responsible for the rise in total histone acetylation after lactate exposure, which
218 was detected by western blot in **figure 3**. Overall, KLa was clearly the most inducible post-
219 translational mofification (PTM) after lactate exposure (**fig S6A)**, and sites that were strongly
220 induced as lactylated were not simultaneously induced as acetylated **(fig S6B)**.
221 In contrast to Kac, major changes did occur in K(me2) and K(me3) after lactate
222 exposure: ~90% of these sites were significantly down-regulated in *P. falciparum* **(fig 6A,**
223 **lower panel; Tables S1-2)**. This was not the case in *P. knowlesi,* where no reciprocal
224 changes in K(me2) and K(me3) were seen.

225 Non-histone chromatin-associated proteins can be lactylated

226 Chromatin-associated proteins besides histones appeared in the mass spectrometry data,
227 and many of these were also lactylated, with a subset of the modifications being induced
228 after exogenous lactate exposure **(Fig 6B, Tables S3-4)**. In *P. falciparum*, lactylated sites
229 were found in chromatin-bound proteins such as Alba3, several RNA helicases, proteins
230 implicated in epigenetics (e.g. histone deacetylase 2), in glycolytic metabolism (e.g. glycerol-
231 3-phosphate dehydrogenase) and in transcriptional control (e.g. two ApiAP2 transcription
232 factors). A third AP2 factor, AP2G, which induces gametocytogenesis, was also detected as

233 lactylated, but its coverage fell below the threshold for inclusion (data not shown), probably
234 due to its very low expression in these asexual-stage cultures. An acetyl-CoA transporter
235 was also lactylated, suggesting again the possibility of cross-talk between acetyl and lactyl
236 epigenetic pathways **(Fig S7A; Table S3)**. In *P. knowlesi*, most of the same proteins were not
237 detected as lactylated, although other proteins, including the acetyltransferase GCN5, were
238 **(Fig S7B; Table S4).**
239 Although almost all the lactylated lysines within histones could also be acetylated
240 **(fig S5B)**, this was not the case in non-histone proteins. Unique, lactate-induced KLa sites
241 appeared on several chromatin-associated proteins. These included epigenetic regulators
242 (e.g. SAP18, associated with HDAC1) and RNA binding proteins such as Alba4 in the case of
243 *P. knowlesi*, and RNA helicases (e.g. NAM7, responsible for RNA turnover), RNA binding
244 proteins, AP2 transcription factors and gametocytogenesis factors (e.g. Male Development
245 1) in the case of *P. falciparum* **(Table S1-2)**.
246 Collectively, it appeared that the KLa modification was widespread, both on histones
247 and on other proteins. It was modulated on some proteins by exogenous lactate, but also
248 probably derived from lactate produced by the parasite. The wide range of lactylated
249 proteins suggests that the modification could regulate multiple aspects of *Plasmodium*
250 biology, from epigenetics to RNA biology to protein function.
251
252 <u>Lactyl post-translational modification does not correlate with levels of protein expression</u>

253 There was no consistent correlation between proteins that were inducibly modified and
254 proteins that changed in abundance after exposure to 25mM lactate (**fig S8**). In *P. knowlesi*,
255 no histones and very few other proteins showed significant changes (with a sca.*P*-value ≤
256 0.01) after lactate exposure; in *P. falciparum*, a few proteins did change significantly in
257 abundance, including histone H2A.Z and HP1, and interestingly the changes were mostly
258 downregulation (**fig S8A**). Overall, however, there was no correlation between proteins
259 whose PTMs were significantly changed, and proteins that changed in abundance (**fig S8B**).
260 Therefore, protein lactylation does not appear to be a consistently 'stabilizing' nor
261 'destabilizing' PTM.

262 <u>Proteins in different biological pathways are lactylated in *P. falciparum* versus *P. knowlesi*</u>

263 It was apparent that the PTMs affected by lactate exposure, both on histones and on non-
264 histone proteins, differed in *P. falciparum* versus *P. knowlesi.* Gene ontology (GO)
265 enrichment analysis was therefore performed to gain insight into the pathways most
266 affected in each species.
267 Amongst the proteins whose PTMs changed after lactate exposure, many different
268 biological functions were found to be enriched *(P*-value ≤ 0.05), depending on both the
269 species and the epigenetic modification (KLa, Kac or Kme). In *P. falciparum,* lactate-
270 modulated KLa sites were significantly enriched in proteins involved with metabolism of

271 tRNAs and indole compounds, for example; in *P. knowlesi,* the top GO terms associated with
272 such KLa sites included 'cell growth', 'cell division' and 'autophagy' **(fig 7A, fig S9, Table S5)**.
273 Amongst GO terms for cellular components, KLa sites, as well as Kac and Kme sites,
274 that responded to lactate exposure were enriched in proteins involved with the nucleosome
275 and protein-DNA complexes. This was not surprising given the known predominance of such
276 PTMs on histones, as well as the location of KLa observed in **figure 4**, which was almost
277 exclusively nuclear. In *P. knowlesi*, there was also an interesting enrichment of lactate-
278 modulated KLa sites in the carbon CCR4/Not complex, which regulates aspects of protein
279 function, RNA metabolism and transcriptional activity during late gametocyte differentiation
280 and post-fertilization development [19] **(fig 7B, fig S10, Table S5).** Amongst molecular
281 function GO terms, both species showed enrichment of 'protein dimerization' and 'catalytic
282 activity', amongst others **(fig S11, Table S5)**.
283
284 <u>Blood lactate levels in malaria-infected mice correlate with distinct transcriptomic profiles in</u>
285 <u>the causative parasites</u>

286 In **figure 1D**, we investigated a rodent malaria model that becomes severely hyperlactaemic,
287 *P. yoelii* 17XL, and showed that histone lactylation in the *P. yoelii* parasites was strongly
288 induced in hyperlactaemic hosts. Using this model, RNAseq analysis had previously been
289 conducted in groups of mice with early-stage versus late-stage infections (i.e. low versus
290 high blood lactate) [14]. We re-analysed those data for the parasite (rather than the host)
291 transcriptome, seeking changes that correlated with high histone lactylation in late-stage
292 infections. For comparison, we analysed the same data from *P. berghei* ANKA, where late-
293 stage infections did not consistently generate hyperlactataemia [14]. Rodent malarias such as
294 these are commonly used as *in vivo* experimental systems, instead of less-accessible human
295 malaria patients, and these existing data offered a valuable resource to suggest biological
296 processes that might be epigenetically affected by lysine lactylation.
297 All datasets were first corrected for different mixes of parasite developmental stages
298 [20], and indeed marked differences in the proportions of schizonts were detected in early
299 versus late-stage *P. yoelii* infections, while gametocytes were found in low proportions in
300 early infections but were undetectable in late infections **(Table S6).**
301 Differential expression (DE) analysis [21] performed on the corrected data revealed
302 distinct expression profiles in late versus early stages of infection in both species **(fig S12A)**.
303 Large cohorts of genes were differentially expressed (*P*-value ≤0.05): 502 genes in *P. yoelii*
304 (238 upregulated and 264 downregulated) and 1521 genes in *P. berghei* (803 upregulated
305 and 718 downregulated) (**fig S12B, Table S6**). (Using more stringent criteria, *P*-value ≤0.05
306 and |log2FC| ≥ 1, expression changes were similarly distributed across fewer total genes **(fig**
307 **S12B)**). Late-stage *P. yoelii* parasites showed a strong downregulation of the lactate
308 dehydrogenase (LDH) gene, as well as the glycolytic enzyme phosphofructokinase (PFK) and
309 several genes putatively involved in gametocytogenesis. Several tRNA synthetases were
310 also downregulated, with the interesting exception of isoleucine tRNA synthetase
311 (isoleucine is the only amino acid that the parasite must scavenge from its host). Indeed,

genes with the strongest expression changes were generally downregulated, while fewer – including several histones – were upregulated **(fig 8A,B)**. The opposite was true in late-stage *P. berghei*, where gene upregulation was most apparent, including the upregulation of phosphofructokinase and glyceraldehyde 3-phosphate dehydrogenase, and factors involved in DNA replication and repair such as MCMs and RecQ helicase **(fig 8A,B)**.

We used chromatin immunoprecipitation (ChIP) to check whether a selection of *P. yoelii* genes that were differentially expressed in hyperlactataemic hosts were also differentially marked with lactyl lysine **(fig 8C, fig S12C)**. Lactylation correlated strongly with blood lactate in the coding sequences of all five chosen genes, which encoded factors involved in gametocytogenesis (AP2G), metabolism (LDH, PFK), etc., whereas there was no correlation in nine control genes without differential expression. Lactylation within 1kb upstream of the same five genes was more variable and less strongly correlated with blood lactate than lactylation within the gene body (**fig S12D**). Thus, it is likely that lactylation of histones and/or other chromatin proteins within gene bodies directly regulates gene transcription, at least in the *P. yoelii* model.

When GO enrichment analysis was conducted on the up- and down-regulated genes, it was clear that late-stage *P. yoelii* parasites activated biological **(fig 8D)** and molecular **(fig S13)** functions including proteolysis and mono-carboxylic acid metabolism, while late-stage *P. berghei* parasites activated contrasting functions including DNA replication and repair, chromosome segregation, cell division and actin/cytoskeleton dynamics. Amongst functional pathways, late-stage *P. yoelii* parasites upregulated fatty acid metabolism whereas *P. berghei* upregulated sugar metabolism and glycolysis **(fig S13).** Thus, it appeared that *P. yoelii* parasites in hyperlactaemic hosts showed features of 'dormancy', which can be induced in *P. falciparum* by isoleucine starvation and is characterised by slowing of the replicative cycle and proteolysis [22]; whereas *P. berghei* – in hosts without hyperlactataemia – conversely upregulated pathways involved in replication.

DISCUSSION

This work represents the first characterisation of a new epigenetic mark, histone lactylation, in the malaria parasite *Plasmodium.* A lactylation epigenetic pathway could be highly influential in the biology and pathology of malaria, because some *Plasmodium* species, including *P. falciparum*, characteristically cause hyperlactataemia in their hosts [3]. It would therefore make sense if these parasites had evolved to sense and respond to hyperlactataemia, potentially modulating their virulence or transmission dynamics. Furthermore, 'epigenetic drugs' such as histone methyltransferase or deacetylase inhibitors have been shown to kill parasites, so epigenetic pathways in general are potential targets for antimalarial drug development [23,24].

Here, we show that histone lysine lactylation in several *Plasmodium* species is rapidly inducible by exogenous lactate, and also rapidly reversible. (These dynamics differ from those reported in mammalian macrophages, where histone lactylation was originally discovered, and where the modification occurred relatively slowly [10].) We detected histone

353 lactylation across four *Plasmodium* species, both *in vitro* and *in vivo*, but it was not equally
354 prominent, nor equally responsive to exogenous lactate, in all species. Rather, it was more
355 abundant and more inducible in species that cause hyperlactataemia: *P. falciparum* and *P.*
356 *yoelii*. In cultured *P. knowlesi*, a species that is only rarely associated with lactic acidosis in
357 humans [25], the modification was less abundant and was not clearly regulated across a
358 normal cell cycle, as it was in *P. falciparum.* In *P. berghei* ANKA, which did not cause
359 consistently high levels of hyperlactataemia in mice, the modification was not clearly
360 responsive to blood lactate, whereas in *P. yoelii* 17XL, it was. Commensurate with profound
361 species-specific differences, mass spectrometry showed that the histone lysine residues
362 lactylated in *P. falciparum* and *P. knowlesi* were generally different.
363
364 In human cells, it has been suggested that lactylation may act like acetylation on
365 histone tails – as a transcription-activating mark [10]. In *Plasmodium*, this may also be true.
366 KLa was detected throughout nuclear chromatin, which is mainly euchromatic, with no
367 specificity for heterochromatin. Furthermore, Kme marks are generally gene-silencing in *P.*
368 *falciparum*, and mass spectrometry showed that these were mostly downregulated after
369 lactate exposure, suggesting reciprocal regulation of KLa-induced activation and Kme-
370 induced silencing. Again, species-specificity was apparent: such reciprocity was notably
371 absent in *P. knowlesi.*
372 KLa and Kac were not, however, interchangeable: only a small subset of Kac sites in
373 either species was detected as lactylated, and a large proportion of the KLa sites, but only a
374 few Kac sites, were induced by exogenous lactate. This has implications for the theory that
375 histone acetyltransferases (HATs), which normally use acetyl-CoA, can also use lactyl-CoA to
376 act as writers of KLa [10]. Since lysine residues were not simply modified with either moiety
377 according to substrate abundance, our results would suggest that only some HATs might use
378 lactyl-CoA, on only some lysine sites. In fact, if conditions of high lactate do stimulate
379 certain HATs towards lactyltransferase activity, the same conditions appear to stimulate
380 acetyltransferase activity on a subset of residues as well, since histone acetylation rose
381 modestly after lactate exposure. The possible contributions of *P. falciparum* HATs to
382 lactyltransferase activity are currently being investigated. An entirely separate pathway was
383 also recently reported, in which alanine tRNA synthetase moonlights as a lactyltransferase
384 [26,27] and this might also operate in *Plasmodium.*
385
386 Besides histone tail lactylation, we detected numerous non-histone proteins being
387 lactylated. These were certainly not comprehensively surveyed because our mass
388 spectrometry focussed on small, chromatin-associated proteins (large, nucleoplasmic or
389 cytoplasmic proteins were probably under-detected). Nevertheless, we detected lactylation
390 on ApiAP2 transcription factors, RNA processing factors, HATs and HDACs amongst others.
391 Unlike the histone tails, where almost every lactylated lysine could also be acetylated, some
392 non-histone proteins were uniquely lactylated (and again, they were largely species-specific
393 between *P. falciparum* and *P. knowlesi*). Thus, the lactyl PTM may have evolved, species-

394 specifically, to regulate *Plasmodium* biology on at least three levels: the epigenetic control
395 of gene transcription via histone tail marks, the co-transcriptional control of RNA processing,
396 and the post-translational modulation of protein activity in HATs, HDACs, etc. – potentially
397 biasing their enzyme activity from acetyl- to lactyl- specificity. The biological pathways that
398 are actually regulated await investigation, because lactylated proteins associated with a
399 wide range of GO terms. Important pathways could potentially include stress-responsive
400 transcriptional programmes controlled by ApiAP2s (possibly including gametocyte
401 conversion, since lactylated ApiAP2G was detected in *P. falciparum*, albeit at a low level),
402 and the expression of *var* genes or other virulence gene families that are epigenetically
403 regulated via HAT/HDAC activity [8].
404 To gain insight into biological changes that can occur in parasites exposed to
405 hyperlactatemia *in vivo*, we analysed transcriptomic data from *P. yoelii* in hyperlactaemic
406 mice. Profound changes were detected, with features of metabolic dormancy – a
407 programme previously reported in *P. falciparum* parasites starved of isoleucine, the only
408 amino acid that malaria parasites cannot gain from haemoglobin catabolism [22]. Starved *P.*
409 *falciparum* parasites slowed their developmental cycle and activated proteolysis: features
410 also seen here in the GO analysis for late-stage *P. yoelii*, but not in late-stage *P. berghei*
411 where the hosts are not generally hyperlactaemic and the parasites do not induce high
412 levels of histone lactylation. Five genes that were differentially expressed in *P. yoelii* during
413 hyperlactataemia were differentially marked with lactyl lysine, strongly suggesting a direct
414 transcription-modulating effect of lactylation – on histones and/or other chromatin
415 proteins. Future work will focus on comprehensive analyses of the transcriptome and
416 epigenome, to establish which transcriptional programmes in parasites exposed to
417 hyperlactataemia are actually epigenetically controlled by histone lactylation, or by
418 lactylation of other chromatin proteins.

419

420 **MATERIAL & METHODS**

421 **Culture and synchronisation of *P. falciparum* and *P. knowlesi***

422 *Plasmodium falciparum* (NF54 strain) and *Plasmodium knowlesi* (A1-H.1 strain) were grown
423 in RPMI 1640 media (Sigma, R4130) with 2.3 g/L sodium bicarbonate, 50 mg/L hypoxanthine
424 (Sigma, H9377) and 25 µg/L gentamicin (Melford Laboratories, G38000-1), supplemented
425 with 5 g/L Albumax II (Invitrogen, 11021037), 10% horse serum (Gibco, 10368902) and 4 g/L
426 glucose for *P. knowlesi*, or with 2.5 g/L Albumax II and 5% human serum for *P. falciparum*.
427 *P. falciparum* and *P. knowlesi* were cultured in human red blood cells (NHS Blood and
428 Transplant) at 4% or 2% haematocrit respectively in 3% oxygen, 5% CO_2 and 92% nitrogen
429 gas mixture at 37°C.
430 For *P. falciparum* synchronization, parasites at ~ 6% parasitaemia were initially
431 synchronised with 5% sorbitol (w/v in water) and allowed to grow to late schizont stage.
432 ML-10 (LifeArc) [28,29] was then added for 2h at a final concentration of 75 nM. Schizonts

433 were purified via a 65% Percoll (GE Healthcare) gradient (v/v in PBS), washed twice with
434 complete media, and allowed to reinvade in 25% haematocrit in 5 ml of complete media in
435 the abovementioned gas mixture at 37°C for 3h with agitation at 220 rpm. 5% sorbitol was
436 then used to remove residual schizonts and produce a tightly synchronised culture (0 to 3
437 hours post invasion (hpi)).
438 For *P. knowlesi* synchronization, parasites at ~ 6% parasitaemia were centrifuged
439 through a 55% Nycodenz gradient (v/v in RPMI) from 100% Nycodenz stock pH 7.5 (27.6%
440 w/v Nycodenz, 5 mM Tris HCl, 3 mM KCl, 0.3 mM $CaNa_2$·EDTA). Ring stages isolated in the
441 bottom layer were allowed to grow to late schizont stage. ML-10 was then added to a final
442 concentration of 150 nM for 2h. Parasites were centrifuged through a second Nycodenz
443 gradient to collect schizonts from the top layer, which were washed twice with complete
444 media and allowed to reinvade as above. A second Nycodenz cleanup was then performed
445 to remove residual schizonts and produce a tightly synchronised culture (0 to 3 hpi).

446 **Growth of *P. yoelii* and *P. berghei***

447 Eight-week-old wild-type female C57BL/6J or CD1 mice were obtained from Charles River
448 Laboratories. All mice were specified pathogen-free, housed in groups of five in individually
449 ventilated cages, and provided ad libitum access to food and water. All experimental
450 protocols and procedures were performed in accordance of the UK Animals (Scientific
451 Procedures) Act (PP8697814), and were approved by the Imperial College Animal Welfare
452 and Ethical Review Board *(*for *P. yoelii)* or the University of Cambridge AWERB (for *P.*
453 *berghei*). The Office of Laboratory Animal Welfare Assurance for the University of
454 Cambridge covers all Public-Health-Service-supported activities involving live vertebrates
455 (no. A5634-01). This study was carried out in compliance with the ARRIVE guidelines
456 (https://arriveguidelines.org/). All studies were in accordance with the Laboratory Animal
457 Science Association's guidelines for good practice. Prior to any experimental interventions,
458 all mice were acclimatized to animal facilities for one week.
459 *P. yoelii* (17XL strain) was serially passaged through C57BL/6J mice, following
460 previously described protocols [14]. Blood was collected via aseptic cardiac puncture from
461 infected donor mice under non-recovery isoflurane anesthesia and diluted in sterile
462 phosphate-buffered saline to achieve the desired parasite concentration. Experimental mice
463 were subsequently infected with 10^6 live parasites via intraperitoneal (i.p.) injection.
464 *P. berghei* (ANKA 2.34 strain) was maintained by serial passage through CD1 mice as
465 in previously described protocols [30]. Experimental mice were pre-treated with 150µl of
466 6mg/ml phenylhydrazine i.p. three days prior to infection, to induce reticulocytosis. Blood
467 from donor mice at 1-5% parasitaemia was collected by cardiac puncture under non-
468 recovery Ketaset/Rompun anaesthesia and used to infected experimental mice by passage
469 of 150µl blood, i.p..
470 Tail capillary blood samples were collected to prepare blood smears for parasitemia
471 assessment and lactate measurement. Parasitemia was quantified through microscopy of
472 thin blood smears stained with 10% Giemsa, following established protocols [14]. Heparinized

473 blood was collected via cardiac puncture under non-recovery anesthesia, into syringes pre-
474 loaded with heparin, and red blood cells were separated from plasma by centrifugation at
475 4,000g for 10 minutes. Levels of lactate in the cardiac blood of each mouse were
476 immediately measured using the Lactate Pro 2 meter (HAB Direct) for *P. yoelii* experiments,
477 or the L-lactic acid (L-Lactate) assay kit (Megazyme K-LATE) for *P. berghei* experiments. Red
478 blood cells were harvested for parasite histone extraction from ten mice per rodent malaria
479 species, of which seven yielded a viable amount of parasite material when infected with *P.*
480 *yoelii* 17XL and five yielded an appropriate amount when infected with *P. berghei* ANKA
481 2.34.

482 **Sodium L-lactate treatment of *P. falciparum* and *P. knowlesi* cultures**

483 For titration experiments, *P. knowlesi* at 12-14 hpi and *P. falciparum* at 24-26 hpi, both at
484 1% parasitaemia, were washed into fresh media and then treated with 0mM, 5mM, 10mM
485 or 25mM sodium L-lactate (Sigma), for 8h (*P. knowlesi*) and 12h (*P. falciparum*).
486 Subsequently, samples were harvested and crude histone extractions were performed (as
487 described below).
488 For timecourse experiments, *P. knowlesi* parasites at 12-14 hpi and *P. falciparum* at
489 24-26 hpi, both at 1% parasitaemia, were treated with 25mM L-lactate for 8h (*P. knowlesi*)
490 and 12h (*P. falciparum*). Samples were harvested at intervals of 2-6 hours between 14-20
491 hpi for *P. knowlesi* and 24-36 hpi for *P. falciparum*. Lactate was then washed off at 20 hpi
492 (*P. knowlesi*) and 36 hpi (*P. falciparum*), and fresh media was added to parasites. Samples
493 were subsequently harvested at further intervals until reinvasion had occurred:32 hpi (for *P.*
494 *knowlesi*) and 44 hpi (for *P. falciparum*). After the wash-off, media was changed every time
495 samples were harvested. Crude histone extractions were performed from each sample.
496 Control experiments were also performed in parallel, where no L-lactate was added, under
497 the same conditions described above.
498 For mass spectrometry on histones from mixed-stage cultures of both species,
499 parasites at a parasitaemia of ~ 6% were washed into fresh media to remove any
500 endogenously-produced lactate and sodium L-lactate (Sigma), dissolved in incomplete
501 media, was added to a final concentration of 25 mM. For mass spectrometry on histones
502 from trophozoites, *P. falciparum* at 24-26 hpi and *P. knowlesi* at 12-14 hpi were treated with
503 sodium L-lactate. Treatments were for 12 and 9h on the two species respectively.

504 **Extraction of *Plasmodium* histones**

505 *P. falciparum* and *P. knowlesi* cultures were collected by centrifugation at 800 *x g* for 5
506 minutes, followed by resuspending the pellet in 1.5 volumes 1X PBS. To release parasites
507 from erythrocytes, saponin was added to a final concentration of 0.1% and incubated on ice
508 for 10 minutes, followed by centrifugation at 12,000 *x g* at 4°C for 10 minutes. Parasite
509 pellets were washed three times by adding ice cold 1X PBS (2 volumes of the saponin lysate)
510 followed by centrifugation at 6000 *x g* for 2 minutes.

511 For *P. yoelii* and *P. berghei,* infected blood obtained by mouse cardiac puncture was
512 placed in 50 mL RPMI HEPES modification media ('schizont media' - no FCS) and spun at 800
513 *xg* for 5 minutes, followed by an RPMI wash and centrifugation at the same speed. To
514 remove host leukocytes, blood was passed through Plasmodipur filters (EuroProxima, 8011)
515 using a syringe, followed by washing the filter with RPMI media to elute any remaining
516 blood. The filtration procedure was repeated a second time before collecting the blood
517 pellet by centrifugation at 800 *xg* for 5 minutes. Filtered blood was then mixed with 0.1 %
518 saponin on ice for 15 minutes to release parasites, which were then collected as above.
519 Parasites from all species were processed either for crude or acid-based histone
520 extraction. For crude histone extraction, parasite cell pellets were lysed by adding 1X RIPA
521 buffer (250 mM Tris-Hcl pH 8.0, 750 mM NaCl, 5% NP-40, 5% sodium deoxycholate, 0.5%
522 SDS, 1mM phenylmethylsulfonyl fluoride, 1X cComplete EDTA-free protease inhibitor
523 cocktail (Roche)) followed by three freeze/thaw cycles on dry ice, 2 minutes each. Laemmli
524 buffer was then added to a final concentration of 1X, boiled at 95 °C for 10 minutes and
525 stored at -80°C for western blot analysis.
526 For mass spectrometry analysis, nuclei were liberated from parasite cell pellets by
527 gently resuspending the parasite pellet twice in two volumes of hypotonic buffer A (10 mM
528 Tris-HCl (pH 8.0), 3 mM $MgCl_2$, 0.2% v/v Nonidet P-40, 0.25 M sucrose, and a cocktail of
529 EDTA-free protease inhibitors (Roche, 0469313200) followed by centrifugation at 4000 x
530 *g* at 4°C for 10 minutes. The resulting chromatin pellet was then resuspended in two
531 volumes of hypotonic buffer B (10 mM Tris-HCl, pH 8.0, 0.8 M NaCl, 1 mM EDTA [including
532 protease inhibitor cocktail]) and incubated on ice for 10 minutes followed by centrifugation
533 at 4000 x *g* at 4°C for 10 minutes. The chromatin pellet was then resuspended with eight
534 volumes of 0.25 M ice-cold HCl followed by vigorous vortexing and rotation for 2h at 4 °C.
535 Acid-soluble recovered proteins in the supernatant were collected by centrifugation at
536 12,000 *x g* for 30 minutes at 4 °C. Histone-containing supernatant was mixed with an equal
537 volume of 30% TCA and incubated overnight rotating at 4 °C, followed by centrifugation at
538 12,000 *x g* for 15 minutes at 4 °C to collect the histone-containing pellet. This was then
539 washed with 500 µl of ice-cold acetone and incubated at -20 °C for 3h, followed by
540 centrifugation at 12,000 *x g* for 15 minutes. Histone pellet was then air-dried and
541 reconstituted in 50 µl ddH_20. Protein concentration was measured using Qubit protein
542 quantification kit (Invitrogen, Q33211). Purity of extracted histones was then assessed by
543 SDS-PAGE on a 15% acrylamide gel stained with Coomassie blue G-250.
544
545 **Western blotting**

546 Protein extracts were loaded on 15% SDS polyacrylamide gels. For lactate-titration blots,
547 approximately 10 µg and 100 µg were loaded for *P. falciparum* and *P. knowlesi* protein
548 extracts respectively. For timecourse blots, up to 100 µg and 200 µg were loaded for *P.*
549 *falciparum* and *P. knowlesi* protein extracts respectively. For validation of histone
550 lactylation prior to mass spectrometry, ~ 10 µg of acid-extracted histones were used. All

551 gels were run at 120 V for 3h and transferred to 0.45 µM nitrocellulose membrane (GE
552 healthcare, 10600020). For both chemiluminescent (**figs 1-3**) and fluorescent (**fig S4**) blots,
553 membranes were blocked in PBS-0.1% Tween 20 containing 5% bovine serum albumin, then
554 probed with designated primary antibodies. For chemiluminescent detection, horseradish
555 peroxidase (HRP)-coupled secondary antibodies were used and developed with ECL Plus
556 Western Chemiluminescent HRP Substrate (ThermoScientific, 11527271). For fluorescent
557 detection, fluorescent secondary antibodies were used. Blots were imaged with an Azure
558 biosystems imager 500 and densitometry was performed with ImageJ for all western blots
559 from titration and timecourse experiments. All lactylated histone signals were normalised
560 using a parallel blot for total histone H4 (except for the fluorescence blot in **figure S4**, where
561 lactylated histones were normalized using the H4 signal on the same blot). To represent
562 data from multiple independent experiments on the same graph, the normalised values for
563 lactylated histones within each experiment were then expressed as a fold change from the
564 control condition (no added lactate in a titration experiment, or time-0 in a timecourse
565 experiment).

566 Antibodies used in western blotting and immunofluorescence microscopy

Primary antibody	**Dilutions**		**Secondary antibody**	**Dilutions**	
	WB	IF		WB	IF
HA - Anti-HA High Affinity Rat mAB 50 ug (Roche 11867423001)		1:500	Alexa Fluor 488-conjugated anti-rat IgG (ThermoFisher A-11006)		1:1000
KLA - Anti-L-Lactyllysine Rabbit mAb 100 ul (PTM-1401)	1:1000 (chemi) 1:10,000 (fluor)	1:500	Alexa Fluor 594-conjugated anti-rabbit IgG (ThermoFisher A-11012) Goat-anti-rabbit IgG IR800 (AzureSpectra, AC2134)	1:10,000	1:1000
H4KL12 - Anti-Lactyl-Histone H4 (Lys12) Rabbit pAB 100 ul (HOLZEL PTM-1411)	1:000	1:500	Alexa Fluor 594-conjugated anti-rabbit IgG (ThermoFisher A-11012)		1:1000
H3ac - Ant-Histone H3ac (pan-acetyl) Rabbit pAb 100 µg (Active motif 61637)	1:4000	1:500	Alexa Fluor 594-conjugated anti-rabbit IgG (ThermoFisher A-11012)		1:1000
H4ac - Anti-Histone H4 (acetyl K5 + K8 + K12) 50 µg (Abcam ab233193)	1:4000	1:500	Alexa Fluor 594-conjugated anti-rabbit IgG (ThermoFisher A-11012)		1:1000

Rabbit anti-histone H4 (Abcam, ab10158)	1:3000	1:500	HRP-conjugated goat anti-rabbit IgG (Abcam, ab6721)	1:2500	1:1000
Mouse anti-histone H4 (Abcam, ab17036)	1:1000 (fluor)		Goat-anti-mouse IgG IR700 (AzureSpectra, AC2129)	1:10,000	

567

568 **Lactate assay**

569 Lactate assays were performed using the L-lactic acid (L-Lactate) assay kit (Megazyme K-
570 LATE). Media samples were taken from 5 ml cultures of *P. falciparum* NF54 and *P. knowlesi*
571 A1-H.1, synchronised with Percoll at the ring stage, starting with 0.5% parasitaemia, every
572 24 h for 5 days. For two biological repeats the cultures were split every 48 h and for
573 another two biological repeats the cultures were not split. The lactate assay was performed
574 according to the manufacturer's instructions (Megazyme K-LATE) on triplicate media
575 samples of 2µl, plated in the 96-well format. The assays were read on a FLUOstar
576 Microplate Reader (BMG LABTECH). Parasitaemia was verified by microscopy every time
577 samples were collected. Results were analysed using GraphPad Prism.

578 **Immunofluorescence assay**

579 Smears were made from *P. falciparum* 3D7 HP1_HA + BSD (gift from Prof Till Voss [17]) and
580 NF54, using mixed stage cultures at 4% parasitaemia. Smears were air dried, fixed in 4%
581 paraformaldehyde/PBS for 10 minutes, washed in PBS, air dried and stored at 4°C. Parasites
582 were permeabilised in 0.2% Triton X-100 for 15 minutes, washed in PBS, and blocked in 1%
583 BSA/PBS with 0.1% Tween-20 for 1 h. Primary antibody labelling was done for 1 h, diluted
584 1:500 in 1% BSA/PBS, followed by three 5-minute washes with block (1% BSA with 0.1%
585 Tween-20). Secondary antibody labelling was done for 1 h, diluted 1:1000 in 1% BSA/PBS,
586 followed by one 5-minute wash with block (see table 1 for antibodies). The slides were then
587 incubated with DAPI (4'6-diamidino-2-phenylindole) (Thermo Fisher Scientific) at 2 µg/mL in
588 PBS for 5 minutes, followed by one 5-minute wash with block. All incubation and labelling
589 steps were done at room temperature. Slides were cured using ProLong Diamond Antifade
590 Mountant (Invitrogen) at room temperature and stored at 4°C prior to visualisation. Slides
591 were imaged using a confocal fluorescence microscope Zeiss LSM700. Images were pseudo-
592 coloured and merged using Fiji-win64 (Image J).

593 **Mass spectrometry**

594 - <u>Sample preparation for mass spectrometry</u>

595 50 µg of acid-extracted histones were resolved on SDS-PAGE 15% acrylamide gel (95 V, 3 h).
596 Gel was stained with QC colloidal Coomassie blue G-250 (Biorad, 1610803) for 3 h, then
597 washed with several changes of nuclease-free water over 1 h. Bands between 10 and 15

598 kDa were then excised and washed with several changes of 50% acetonitrile for destaining,
599 followed by 100% acetonitrile. Gel plugs were then incubated in 0.05 M NH_4HCO_3 and 10
600 mM DTT at 56 °C for 45 minutes for disulphide bond reduction, and with 55 mM
601 iodoacetamide and 0.1 M NH_4 for alkylation, followed by treatment with iodoacetamide for
602 30 min at 30 °C in the dark. Gel plugs were then washed with water and 50% acetonitrile.
603 For dehydration, 100% acetonitrile was added, followed by rehydration in 50 mM NH_4HCO_3
604 containing 12.5 ng/µL trypsin (Promega modified trypsin). Samples were incubated
605 overnight at 37 °C. After digestion, the supernatant was pipetted into a sample vial and
606 loaded onto an autosampler for automated LC-MS/MS analysis.

607 - Reverse phase chromatography and mass spectrometry

608 All LC-MS/MS experiments were performed using a Dionex Ultimate 3000 RSLC nanoUPLC
609 system (Thermo Fisher Scientific Inc, Waltham, MA, USA) and a Q Exactive Orbitrap mass
610 spectrometer (Thermo Fisher Scientific Inc, Waltham, MA, USA). Separation of peptides was
611 performed by reverse-phase chromatography at a flow rate of 300 nL/min and a Thermo
612 Scientific reverse-phase nano Easy-spray column (Thermo Scientific PepMap C18, 2mm
613 particle size, 100A pore size, 75 mm i.d. x 50cm length). Peptides were loaded onto a pre-
614 column (Thermo Scientific PepMap 100 C18, 5mm particle size, 100A pore size, 300 mm i.d.
615 x 5mm length) from the Ultimate 3000 autosampler with 0.1% formic acid for 3 minutes at a
616 flow rate of 15 mL/min. After this period, the column valve was switched to allow elution of
617 peptides from the pre-column onto the analytical column. Solvent A was water + 0.1%
618 formic acid and solvent B was 80% acetonitrile, 20% water + 0.1% formic acid. The linear
619 gradient employed was 2-40% B in 90 minutes. Further wash and equilibration steps gave a
620 total run time of 120 minutes.
621 The LC eluant was sprayed into the mass spectrometer by means of an Easy-Spray
622 source (Thermo Fisher Scientific Inc.). All m/z values of eluting ions were measured in an
623 Orbitrap mass analyzer, set at a resolution of 35000 and was scanned between m/z 380-
624 1500. Data dependent scans (Top 20) were employed to automatically isolate and generate
625 fragment ions by higher energy collisional dissociation (HCD, NCE:26%) in the HCD collision
626 cell and measurement of the resulting fragment ions was performed in the orbitrap
627 analyser, set at a resolution of 17500. Singly charged ions and ions with unassigned charge
628 states were excluded from being selected for MS/MS and a dynamic exclusion window of 40
629 was employed.
630

631 - Data processing, protein quantification and PTM localisation

632 For all experiments, raw mass spectrometry data were analyzed using MaxQuant [31] v.
633 1.5.0.0 by employing Andromeda for MS/MS spectra search against the *P. falciparum* and *P.*
634 *knowlesi* PlasmoDB FASTA proteome reference (release 64), and a common contaminant
635 database [32]. In MaxQuant, enzyme specificity was set to Trypsin/P; carbamylation of
636 cysteines was set as a fixed modification and Acetyl lysine, lactyl lysine, and di/tri methyl

637 lysine, as variable modifications. Missed cleavage sites were set to 5 with a maximum
638 number of 3 modifications per peptide. For protein quantification, major protein
639 aggregation was changed to sum. Match between run was turned on. PTMs quantification
640 files generated by MaxQuant were exported to Perseus (v3.6.2) [33] to collapse localisation
641 site information and remove reverse and contaminants. For all PTMs, sites were identified in
642 both conditions for mixed-stage experiments, or in at least two replicates per condition for
643 trophozoites. Remaining protein quantification and PTM quantification steps were
644 performed in R (v3.6.2) as described below.

645 - Downstream data analysis for differential protein and PTM expression

646 For all experiments, PTM peptide quantification files obtained after Perseus filtering steps
647 described above, and ProteinGroup.txt protein quantification files obtained by MaxQuant,
648 were exported to R for further processing. For mixed-stage experiments, $\log_2$ transformed
649 PTM intensities were normalised using quantile normalisation using the
650 normalizeBetweenArrays function from limma package (v3.42) [34]. For trophozoite-stage
651 experiments, $\log_2$ transformed PTM intensities were normalised using quantile and VSN
652 normalisation for *P. falciparum* and *P. knowlesi*, respectively, using the
653 normalizeBetweenArrays function from limma package (v3.42). VSN was chosen for the
654 latter due to technical variability between biological replicates, which affected replicate 1
655 only from both + and - lactate conditions. Imputation of missing values was done by low-
656 rank approximation of the normalised PTM data matrix using msImpute [35]. In brief,
657 imputation was performed with V2 method if values were missing at random, or by
658 Barycenter approach if missingness was not at random. Differentially expressed sites were
659 calculated using limma (two-sided, BH p value < 5%). At the protein level, reverse and
660 contaminants were removed from ProteinGroup.txt quantification file, followed by
661 extracting LFQ intensities and requiring at least two values per condition. For better
662 accuracy in global protein levels, spectraCounteBayes function from DEqMS package
663 (v1.22.0) [36] was used to make limma's empirical-Bayesian variance calculation dependent on
664 the number of detected peptides/PTMs per protein generated by MaxQuant, rather than
665 estimating a fixed prior distribution for all proteins. Finally, differentially expressed proteins
666 were calculated using limma (two-sided, BH FDR < 1%).

667 **RNA-seq data analysis**

668 Raw reads from the RNA-Seq experiment generated by [14], belonging to Py17XL and PbANKA
669 early and late infection stages, were downloaded, trimmed and quality checked by
670 Trimmomatic v.0.35 [37]. Low quality reads with Phred quality score values lower than 30 and
671 lengths less than 20 bp were removed.
672 (https://www.bioinformatics.babraham.ac.uk/projects/fastqc/). Filtered reads were further
673 quality controlled by FastQC v.0.11.7
674 (https://www.bioinformatics.babraham.ac.uk/projects/fastqc/) and used for transcript
675 quantification using SALMON v.0.82 [38]. Py17XL and PbANKA reference transcript datasets

676 were indexed using the quasi-mapping mode (--type quasi) of Salmon to create k-mers of
677 lengths 31 (-K 31). For transcript quantification, input data sequence bias correction and
678 bootstrapped abundance estimate were performed using the "seqBias" and "nom-
679 Bootstraps 30" parameters from Salmon, respectively. Read counts and transcript per
680 million reads (TPMs) were generated using tximport R package version 1.10.0 and
681 lengthScaledTPM method [39] with inputs of transcript quantifications from tool SALMON.
682 Low-expressed transcripts and genes were filtered based on analysing the data mean-
683 variance trend. The expected decreasing trend between data mean and variance was
684 observed when expressed transcripts were determined as those that had 3 of the 6 samples
685 with count per million reads (CPM) 1, which provided an optimal filter for low expression. A
686 gene was considered to be expressed if any of its transcripts with the above criteria was
687 expressed. The TMM method was used to normalise the gene and transcript read counts to
688 –CPM [40].
689 Prior to DE analysis and to control for heterogeneity within parasite developmental
690 stages, we performed parasite stage deconvolution as follows. A signature matrix was taken
691 from [20], which contains CPM-normalised gene expression measurements calculated across
692 different parasite stages (male and female gametocyte, trophozoite, ring, merozoite, and
693 schizont stages). *P. berghei* and *P. yoelii* gene names were converted to one-to-one
694 orthologous *P. falciparum* gene names using an orthologous gene file obtained from the
695 Malaria Cell Atlas. CPM-normalised counts alongside the signature matrix were then
696 uploaded to CIBERSORT for deconvolution analysis using 100 permutations and disabling
697 quantile normalisation (as recommended by CIBERSORT) to obtain the parasites cell
698 proportions. This was performed separately for reads mapping to *P. berghei* and *P. yoelii*.
699 For DE analysis, limma suite was used [34,41] by fitting a linear model accounting for the
700 cell proportions obtained in CIBERSORT. To compare the expression changes between
701 conditions of experimental design, the contrast groups were set as Late-Early. For DE
702 genes/transcript, the fold change of gene/transcript abundance were calculated based on
703 contrast groups and significance of expression changes were determined using t-test. P-
704 values of multiple testing were adjusted with BH to correct false discovery rate (FDR) [42]. A
705 gene/transcript was considered significantly DE in a contrast group if it had adjusted p-value
706 < 0.01 and $|\log2FC| \geq 1$.

707 **Gene ontology (GO) pathway enrichment analysis**

708 For RNA-Seq datasets, functional GO and pathway enrichment analysis were performed on
709 significantly DE genes only, using PlasmoDB database [43] for annotation with default
710 parameters. The GO terms (biological process, molecular function and cellular component)
711 and pathways were identified to provide biological insights into the significance of DE using
712 a *P-value* ≤ 0.05. For visualization of GO and pathways terms, combined with their
713 associated gene expression profiles/significance, GOPlot R package v.1.02 was used [44].
714 For mass-spectrometry, functional GO enrichment analysis was performed using
715 PlasmoDB database for annotation, with default parameters, on significantly differential

716 proteins of the acid-extracted proteome and PTMs (for the trophozoite-stage experiment
717 only). Exceptionally, for the KLa PTM, GO enrichment analysis was performed on both
718 significantly and non-significantly changing lactylated proteins. Bubble plots were
719 generated using GO terms combined with their associated genes expression
720 profiles/significance across all PTMs and the acid-extracted proteome via in-house R scripts.
721 For both datasets,

722 $$\text{Z-score} = \frac{(Up-Down)}{\sqrt{Count}}$$

723 Where *up* and *down* are the number of genes up-regulated (logFC>0) in the data or down-
724 regulated (logFC<0), respectively.
725
726 **Chromatin immunoprecipitation (ChIP) and quantitative PCR (qPCR)**
727
728 Blood was harvested from three mice infected with *P. yoelii 17XL* at different levels of
729 parasitemia and lactatataemia. Purification of erythrocytes from host leukocytes and
730 release of parasites were performed as described above. Parasites were crosslinked
731 immediately with 1% paraformaldehyde (Sigma) by rotating for 10 mins at 37°C, then
732 quenching with 0.125 M glycine for 5 mins at room temperature. Nuclei were liberated by
733 gently resuspending the parasite pellet twice in two volumes of hypotonic buffer A (10 mM
734 Tris-HCl (pH 8.0), 3 mM $MgCl_2$, 0.2% v/v Nonidet P-40, 0.25 M sucrose, EDTA-free protease
735 inhibitors (Roche, 0469313200)) and holding on ice for 15 mins. This was followed by 15
736 strokes using a dounce homogenizer and centrifugation at 4000 x g at 4°C for 10 mins. The
737 chromatin pellet was then resuspended in two volumes of hypotonic buffer B (10 mM Tris-
738 HCl, pH 8.0, 0.8 M NaCl, 1 mM EDTA, protease inhibitor cocktail) and incubated on ice for 10
739 mins followed by centrifugation at 4000 x g at 4°C for 10 mins. 2-3 µg of chromatin were
740 resuspended in 50 µl of shearing buffer (1% SDS, 50 mM Tris pH 8.0, 10 mM EDTA, 1X
741 protease inhibitor cocktail) and sheared for 47 mins using an M220 sonicator (Covaris) at 5%
742 duty cycle, 200 cycles per burst, and 75 W of peak incident power to generate 150-400 bp
743 fragments.
744 Sheared chromatin was diluted 2x in ChIP dilution buffer (0.01% SDS, 1.1% Triton X-
745 100, 1.2 mM EDTA pH 8.0, 25 mM Tris HCL pH 8.1, 150 mM NaCl, 1X protease inhibitor
746 cocktail) and pre-cleared by incubating with protein A agarose beads (Thermoscientific,
747 20365) for 1 h at 4°C. 10% of the cleared chromatin was reserved as the input control and
748 90% was incubated for 4 h at 4°C using 0.75 µg of anti-KLa antibody coupled with protein A
749 agarose beads. After one wash with low salt buffer (0.1 %SDS, 1% Triton X-100, 2 mM EDTA,
750 20 mM Tris-HCL pH 8.1, 150 mM NaCl), one with high salt buffer (0.1% SDS, 1% Triton X-100,
751 2 mM EDTA pH 8.0, 20 mM Tris-HCl pH 8.0, 500 mM NaCl), and one with lithium chloride
752 (0.25 M LiCl, 1% NP-40, 1% sodium deoxycholate, 1 mM EDTA, 10 mM Tris-HCl pH 8.1), the
753 immunoprecipitate was eluted twice in 85 µl elution buffer (1% SDS, 0.1M $NaHCO_3$) by
754 rotation at 65°C. ChIPed and input DNA were incubated with 2 µg RNase A (Roche,
755 10109169001) at 37°C for 30 min with gentle shaking. Samples were then resuspended in

756 decrosslinking buffer (150 mM NaCl, 0.2% SDS, 600 µg Proteinase K (Ambion, AM2546)) by
757 incubation at 65°C for 3 h with interval shaking. DNA was purified overnight at -20 °C by
758 adding 0.1 volume of 3M sodium acetate, 4 µl of linear polyacrylamide (Ambion, AM9520)
759 and 2.5 volumes of ice cold ethanol, and collected by centrifugation at 13,000 xg for 30 mins
760 at 4°C. DNA pellets were washed once with 70% ice cold ethanol and resuspended in 20 µl
761 of nuclease free water.
762 qPCR was conducted with 3-4 ng of DNA in technical duplicate, using a
763 QuantStudio™ 6 Pro Real-Time PCR System: 2 mins denaturation at 95°C, 40 cycles of 5s
764 95°C, 30s 60°C. Data were presented as the percentage of DNA immunoprecipitated
765 relative to input (100*2^(Ct_{input}-$Ct_{eluates}$)) . Primers were designed in the CDS and within 1kb
766 upstream of the TSS using Primer3 and are listed below.
767

	Target gene name and ID	name	sequence
Significantly regulated CDS	Histone H4 (PY17X_0944400)	Fw	GAAAGGGAGGAGCAAAGAGACATAG
		Rev	CCAGAGATACGTTTAACACCACCTC
	Lactate dehydrogenase, LDH (PY17X_1345100)	Fw	AACCCAGTTGATTGCATGGC
		Rev	CCTTGAACATCACCAGGGTTTAC
	ATP-dependent 6-phosphofructokinase, PFK11 (PY17X_0922000)	Fw	GCAGGAATAGCTGTTGAAAATAATTTGG
		Rev	ATTCTGATTGTTTATAAAATAATACCCGGG
	AP2 domain transcription factor, AP2-G (PY17X_1440000)	Fw	ATTGTGCCGAAACAGTACCG
		Rev	AGCTAACCCGTTGCAATTGG
	isoleucine--tRNA ligase, Ile-tRNA (PY17X_1442500)	Fw	CGACGCTGGATATAAACGAGAATAATG
		Rev	AACAAACCCATAGCCTCACAATATC
Significantly regulated 5'UTR	Histone H4 (PY17X_0944400)	Fw	AAAGTGATGATAATGCATAAATTCGC
		Rev	GAGTTTTGAGTCGATTTTATTTTAAATGGC
	Lactate dehydrogenase, LDH (PY17X_1345100)	Fw	CATACTCAAATGTGTACGTGCA
		Rev	AAATAAAAGCCCAATGACAAGAAAG
	ATP-dependent 6-phosphofructokinase, PFK11 (PY17X_0922000)	Fw	TTAGCGCTATAAACAAGTTACAGCA
		Rev	GCACCTGTAAATAATATATCCAATATGTAC
	AP2 domain transcription factor, AP2-G (PY17X_1440000)	Fw	ATTGTGCCGAAACAGTACCG
		Rev	AGCTAACCCGTTGCAATTGG
	isoleucine--tRNA ligase, Ile-tRNA (PY17X_1442500)	Fw	CTTCTTTAATTTGATGCGACATGAAATC
		Rev	GATTGTACAGAAAAGGGGAGGG
Not significantly regulated CDS	PIR protein (PY17X_0900055)	Fw	AAGGAACGTGATTACCAATTCG
		Rev	TGCCTCCGTTTCAAACACAG
	amino acid transporter, AAT1 (PY17X_1129800)	Fw	CAATTCCATTAAATTTTATTGCGACCTATC
		Rev	ATTTTCTTTGAAACATATCATCTCCTTGAG
	microsomal signal peptidase, MSPase (PY17X_1420400)	Fw	TAAAAGAGGTGATGTTGTATTGCTAATATC
		Rev	TACTATCAAAAGAATCCAGTTTATTATCGC
	apical polar ring protein, APR1 (PY17X_0909100)	Fw.1	CAGGGAAAAGAAGATAAAGATGGGTTAGAC
		Rev.1	CATCAGATTCGGTCATATAATAATGTTCTTC
	apical polar ring protein, APR1 (PY17X_0909100)	Fw.2	AATAAAAGCGATGAGGAATATGAAGACAAC
		Rev.2	TTTCGCTTCTACCTATGTTATATAATTCGC

	golgi protein 1, PRP2 (PY17X_1420000)	Fw	CGTGGAGTAAGTGGAAGATGG
		Rev	TGTCCTTCATCTGCCAAATAGC
	mitochondrial import inner membrane translocase subunit, TIM10 (PY17X_0609600)	Fw	TAGAAGAATGCAAAATTCATGTTGGG
		Rev	ATGAACACATCTATCAACACAACTC
	GPI-anchor transamidase, GPI8 (PY17X_0921600)	Fw	GATCAAAATGTTATCTTTTACGATTCAACC
		Rev	GTAATAGCTTCGATCGTTGTATAAACTTTC
	parasite-infected erythrocyte surface protein, PIESP1 (PY17X_0411000)	Fw	AAGGTATGTTCATTGGATATGGATTTAATG
		Rev	TTGCATCCAAACATGTATTTTCAAAATGAG

ACKNOWLEDGEMENTS

We acknowledge the Cambridge Centre for Proteomics for mass spectrometry; the staff of Imperial College Central Biomedical Services for support with animal experiments; Till Voss (Swiss TPH) for the HP1-HA parasite line; and Rachana Ramarao and Anders Jensen for early work on this project.

FUNDING

This work was funded by Wellcome Discovery Award 225171/Z/22/Z to CJM.
AG is supported by an Imperial College Research Fellowship.
AMB is funded by the MRC [MR/N00227×/1 and MR/W025701/1], Sir Isaac Newton Trust, Alborada Fund, Wellcome Trust ISSF and University of Cambridge JRG Scheme, GHIT, Rosetrees Trust (G109130) and the Royal Society (RGS/R1/201,293 and IEC/R3/19,302).

DATA AVAILABILITY

Sequencing data from mouse, *P.yoelii* and *P. berghei* are available at ENA under the ID PRJEB43641 as per Georgiadou *et al*. [14]. Proteome data are deposited at the ProteomeXchange Consortium via the PRIDE partner with dataset identifier PXD055236. Source data are provided with this paper.

REFERENCES

1 Merrick, C. J. *et al.* Epigenetic dysregulation of virulence gene expression in severe Plasmodium falciparum malaria. *The Journal of infectious diseases* **205**, 1593-1600, doi:10.1093/infdis/jis239 (2012).

2 Krishna, S. *et al.* Lactic acidosis and hypoglycaemia in children with severe malaria: pathophysiological and prognostic significance. *Transactions of the Royal Society of Tropical Medicine and Hygiene* **88**, 67-73, doi:10.1016/0035-9203(94)90504-5 (1994).

3 Possemiers, H., Vandermosten, L. & Van den Steen, P. E. Etiology of lactic acidosis in malaria. *PLoS pathogens* **17**, e1009122, doi:10.1371/journal.ppat.1009122 (2021).

4 Andrade, C. M. *et al.* Increased circulation time of Plasmodium falciparum underlies persistent asymptomatic infection in the dry season. *Nature medicine* **26**, 1929-1940, doi:10.1038/s41591-020-1084-0 (2020).

802 5 Mancio-Silva, L. *et al.* Nutrient sensing modulates malaria parasite virulence. *Nature* **547**,
803 213-216, doi:10.1038/nature23009 (2017).
804 6 Harris, C. T. *et al.* Sexual differentiation in human malaria parasites is regulated by
805 competition between phospholipid metabolism and histone methylation. *Nat Microbiol* **8**,
806 1280-1292, doi:10.1038/s41564-023-01396-w (2023).
807 7 Diffendall, G. *et al.* RNA polymerase III is involved in regulating Plasmodium falciparum
808 virulence. *eLife* **13**, doi:10.7554/eLife.95879.2

809 (2024).
810 8 Duraisingh, M. T. & Horn, D. Epigenetic Regulation of Virulence Gene Expression in Parasitic
811 Protozoa. *Cell host & microbe* **19**, 629-640, doi:10.1016/j.chom.2016.04.020 (2016).
812 9 West, R. & Sullivan, D. J. Lactic acid supplementation increases quantity and quality of
813 gametocytes in Plasmodium falciparum culture. *Infection and immunity* **15**, e00635-00620,
814 doi:10.1128/IAI.00635-20 (2020).
815 10 Zhang, D. *et al.* Metabolic regulation of gene expression by histone lactylation. *Nature* **574**,
816 575-580, doi:10.1038/s41586-019-1678-1 (2019).
817 11 Dai, E., Wang, W., Li, Y., Ye, D. & Li, Y. Lactate and lactylation: Behind the development of
818 tumors. *Cancer Lett* **591**, 216896, doi:10.1016/j.canlet.2024.216896 (2024).
819 12 Su, J. *et al.* Functions and mechanisms of lactylation in carcinogenesis and
820 immunosuppression. *Front Immunol* **14**, 1253064, doi:10.3389/fimmu.2023.1253064 (2023).
821 13 Merrick, C. J. Histone lactylation: a new epigenetic axis for host-parasite signalling in
822 malaria? *Trends Parasitol* **39**, 12-16, doi:10.1016/j.pt.2022.10.004 (2023).
823 14 Georgiadou, A. *et al.* Comparative transcriptomic analysis reveals translationally relevant
824 processes in mouse models of malaria. *Elife* **11**, doi:10.7554/eLife.70763 (2022).
825 15 Hikosaka, K., Hirai, M., Komatsuya, K., Ono, Y. & Kita, K. Lactate retards the development of
826 erythrocytic stages of the human malaria parasite Plasmodium falciparum. *Parasitol Int* **64**,
827 301-303, doi:10.1016/j.parint.2014.08.003 (2015).
828 16 Duffy, S. & Avery, V. M. Routine In Vitro Culture of Plasmodium falciparum: Experimental
829 Consequences? *Trends Parasitol* **34**, 564-575, doi:10.1016/j.pt.2018.04.005 (2018).
830 17 Flueck, C. *et al.* Plasmodium falciparum heterochromatin protein 1 marks genomic loci linked
831 to phenotypic variation of exported virulence factors. *PLoS pathogens* **5**, e1000569 (2009).
832 18 Trelle, M. B., Salcedo-Amaya, A. M., Cohen, A. M., Stunnenberg, H. G. & Jensen, O. N. Global
833 histone analysis by mass spectrometry reveals a high content of acetylated lysine residues in
834 the malaria parasite Plasmodium falciparum. *J Proteome Res* **8**, 3439-3450,
835 doi:10.1021/pr9000898 (2009).
836 19 Hart, K. J., Power, B. J., Rios, K. T., Sebastian, A. & Lindner, S. E. The Plasmodium NOT1-G
837 paralogue is an essential regulator of sexual stage maturation and parasite transmission.
838 *PLoS biology* **19**, e3001434, doi:10.1371/journal.pbio.3001434 (2021).
839 20 Tebben, K., Dia, A. & Serre, D. Determination of the Stage Composition of Plasmodium
840 Infections from Bulk Gene Expression Data. *mSystems* **7**, e0025822,
841 doi:10.1128/msystems.00258-22 (2022).
842 21 Calixto, C. P. G. *et al.* Rapid and Dynamic Alternative Splicing Impacts the Arabidopsis Cold
843 Response Transcriptome. *Plant Cell* **30**, 1424-1444, doi:10.1105/tpc.18.00177 (2018).
844 22 Babbitt, S. E. *et al.* Plasmodium falciparum responds to amino acid starvation by entering
845 into a hibernatory state. *Proceedings of the National Academy of Sciences of the United*
846 *States of America* **109**, E3278-3287, doi:10.1073/pnas.1209823109 (2012).
847 23 Wang, M. *et al.* Drug Repurposing of Quisinostat to Discover Novel Plasmodium falciparum
848 HDAC1 Inhibitors with Enhanced Triple-Stage Antimalarial Activity and Improved Safety.
849 *Journal of medicinal chemistry* **65**, 4156-4181, doi:10.1021/acs.jmedchem.1c01993 (2022).
850 24 Malmquist, N. A., Moss, T. A., Mecheri, S., Scherf, A. & Fuchter, M. J. Small-molecule histone
851 methyltransferase inhibitors display rapid antimalarial activity against all blood stage forms

852 in Plasmodium falciparum. *Proceedings of the National Academy of Sciences of the United*
853 *States of America* **109**, 16708-16713, doi:10.1073/pnas.1205414109 (2012).
854 25 Barber, B. E., Grigg, M. J., William, T., Yeo, T. W. & Anstey, N. M. The Treatment of
855 Plasmodium knowlesi Malaria. *Trends Parasitol* **33**, 242-253, doi:10.1016/j.pt.2016.09.002
856 (2017).
857 26 Ju, J. *et al.* The alanyl-tRNA synthetase AARS1 moonlights as a lactyltransferase to promote
858 YAP signaling in gastric cancer. *J Clin Invest* **134**, doi:10.1172/JCI174587 (2024).
859 27 Zong, Z. *et al.* Alanyl-tRNA synthetase, AARS1, is a lactate sensor and lactyltransferase that
860 lactylates p53 and contributes to tumorigenesis. *Cell* **187**, 2375-2392 e2333,
861 doi:10.1016/j.cell.2024.04.002 (2024).
862 28 Large, J. M. *et al.* Potent bicyclic inhibitors of malarial cGMP-dependent protein kinase:
863 approaches to combining improvements in cell potency, selectivity and structural novelty.
864 *Bioorg Med Chem Lett* **29**, 126610, doi:10.1016/j.bmcl.2019.08.014 (2019).
865 29 Large, J. M. *et al.* Potent inhibitors of malarial P. Falciparum protein kinase G: Improving the
866 cell activity of a series of imidazopyridines. *Bioorg Med Chem Lett* **29**, 509-514,
867 doi:10.1016/j.bmcl.2018.11.039 (2019).
868 30 Blagborough, A. M. *et al.* Transmission-blocking interventions eliminate malaria from
869 laboratory populations. *Nature communications* **4**, 1812, doi:10.1038/ncomms2840 (2013).
870 31 Cox, J. & Mann, M. MaxQuant enables high peptide identification rates, individualized p.p.b.-
871 range mass accuracies and proteome-wide protein quantification. *Nat Biotechnol* **26**, 1367-
872 1372, doi:10.1038/nbt.1511 (2008).
873 32 Cox, J. *et al.* Andromeda: a peptide search engine integrated into the MaxQuant
874 environment. *J Proteome Res* **10**, 1794-1805, doi:10.1021/pr101065j (2011).
875 33 Tyanova, S. *et al.* The Perseus computational platform for comprehensive analysis of
876 (prote)omics data. *Nature methods* **13**, 731-740, doi:10.1038/nmeth.3901 (2016).
877 34 Ritchie, M. E. *et al.* limma powers differential expression analyses for RNA-sequencing and
878 microarray studies. *Nucleic acids research* **43**, e47, doi:10.1093/nar/gkv007 (2015).
879 35 Hediyeh-Zadeh, S., Webb, A. I. & Davis, M. J. MsImpute: Estimation of Missing Peptide
880 Intensity Data in Label-Free Quantitative Mass Spectrometry. *Mol Cell Proteomics* **22**,
881 100558, doi:10.1016/j.mcpro.2023.100558 (2023).
882 36 Zhu, Y. *et al.* DEqMS: A Method for Accurate Variance Estimation in Differential Protein
883 Expression Analysis. *Mol Cell Proteomics* **19**, 1047-1057, doi:10.1074/mcp.TIR119.001646
884 (2020).
885 37 Bolger, A. M., Lohse, M. & Usadel, B. Trimmomatic: a flexible trimmer for Illumina sequence
886 data. *Bioinformatics* **30**, 2114-2120, doi:10.1093/bioinformatics/btu170 (2014).
887 38 Patro, R., Duggal, G., Love, M. I., Irizarry, R. A. & Kingsford, C. Salmon provides fast and bias-
888 aware quantification of transcript expression. *Nature methods* **14**, 417-419,
889 doi:10.1038/nmeth.4197 (2017).
890 39 Soneson, C., Matthes, K. L., Nowicka, M., Law, C. W. & Robinson, M. D. Isoform prefiltering
891 improves performance of count-based methods for analysis of differential transcript usage.
892 *Genome biology* **17**, 12, doi:10.1186/s13059-015-0862-3 (2016).
893 40 Bullard, J. H., Purdom, E., Hansen, K. D. & Dudoit, S. Evaluation of statistical methods for
894 normalization and differential expression in mRNA-Seq experiments. *BMC bioinformatics* **11**,
895 94, doi:10.1186/1471-2105-11-94 (2010).
896 41 Law, C. W., Chen, Y., Shi, W. & Smyth, G. K. voom: Precision weights unlock linear model
897 analysis tools for RNA-seq read counts. *Genome biology* **15**, R29, doi:10.1186/gb-2014-15-2-
898 r29 (2014).
899 42 Benjamini, Y. & Yekutieli, D. Quantitative trait Loci analysis using the false discovery rate.
900 *Genetics* **171**, 783-790, doi:10.1534/genetics.104.036699 (2005).
901 43 Aurrecoechea, C. *et al.* PlasmoDB: a functional genomic database for malaria parasites.
902 *Nucleic acids research* **37**, D539-543, doi:10.1093/nar/gkn814 (2009).

44 Walter, W., Sanchez-Cabo, F. & Ricote, M. GOplot: an R package for visually combining expression data with functional analysis. *Bioinformatics* **31**, 2912-2914, doi:10.1093/bioinformatics/btv300 (2015).

908 **FIGURE LEGENDS**

909 1. *Plasmodium* histones are inducibly lactylated

910 A, B: Lysine lactylation was measured in *P. falciparum* parasites grown in different
911 concentrations of L-lactate for 12h. Western blots show 'Pan KLa'(A) and histone H4 K12
912 lactylation ('H4K12La', (B)), as well as total histone H4 as a control. Graphs show
913 quantifications of blots from several independent experiments (n=4 for PanKLa, n=3 for
914 H4K12La) with each lactyl-histone signal quantified relative to histone H4, then expressed
915 as a fold-change from the 0mM condition (bars show means, dots show individual values,
916 error bars show SEM). Multiple comparison of means was performed using one-way
917 ANOVA and Tukey HSD post hoc test: *, $p < 0.05$; ***, $p < 0.001$; comparisons not shown,
918 not significant. A representative western blot from each group of experiments is shown.

919 C, D: Lysine lactylation was measured in *P. knowlesi* parasites grown in different
920 concentrations of L-lactate for 8h, as in (A, B).

921 E: Lysine lactylation was measured in *P. yoelii* 17XL parasites exposed to varying levels of
922 lactate in the blood of the host mouse. Western blots show 'Pan KLa' and histone H4 as
923 control. M1-M7, individual mice. Scatter plot represents Pearson correlation (R^2= 0.56)
924 between histone KLa signal intensities normalized to H4 (*y*-axis) and lactate levels in the
925 blood (*x*-axis) upon parasite collection from the host.

926

927 2. Histone lactylation is rapidly inducible and reversible

928 A: Lysine lactylation ('Pan KLa') measured in *P. falciparum* parasites grown for 12h from the
929 early trophozoite stage either in 25mM L-lactate (+Lac), or in control media without
930 added lactate (Control). Parasites were then washed into fresh media. Samples were
931 taken for western blotting at intervals from 0 to 24h. Stage of the parasite culture is
932 shown on the x-axis: ET, early trophozoite; MT, mid trophozoite; LT, late trophozoite; S,
933 schizont; R, ring. Graph shows data (mean and range) from two independent timecourse
934 experiments, each quantified as fold-changes from time-0 in the signal of KLa versus
935 total-H4, with one representative western blot shown.

936 B: Lysine lactylation ('Pan KLa') measured in *P. knowlesi* parasites grown for 8h from the
937 early trophozoite stage either in 25mM L-lactate, or in control media without added
938 lactate, then washed into fresh media. Samples were taken for western blotting at
939 intervals from 0 to 20h. Stage of the parasite culture is shown on the x-axis as in A; data
940 were quantified and represented as in (A).

941 C,D: Lactate levels and parasitaemias were measured every 24h in cultures of *P. falciparum*
942 (C) and *P. knowlesi* (D), starting at 0.5% parasitaemia, either split back to 0.5% every 48h
943 or allowed to grow continuously without splitting. Data shown are the mean of biological
944 duplicate experiments.

945 E: *P. falciparum* parasites were grown from 1% parasitaemia without splitting or changing
946 the media for 72h, starting at the early-trophozoite stage and sampling every 12h. Stage
947 of the parasite culture is shown on the x-axis as in A, and example parasite morphology is

948 also shown. By 60h, morphology showed that the culture was starting to crash, with
949 dead (D) pyknotic parasites by 72h. The graph shows fold-changes in KLa signal from
950 time-0, quantified from biological duplicate experiments, as in (A,B); one representative
951 western blot is shown.
952
953 3. Histone acetylation is affected by exposure to high lactate
954 A,B: Histone 3 lysine acetylation ('H3Kac', (A)) and histone 4 lysine acetylation ('H4Kac', (B))
955 were measured in *P. falciparum* parasites grown in different concentrations of L-lactate
956 for 12h, as in figure 1. Graphs show quantification of blots from several independent
957 experiments (n=3) with each acetyl-histone signal quantified relative to histone H4, then
958 expressed as a fold-change from the 0mM condition (bars show means, dots show
959 individual values, error bars show SEM). Multiple comparison of means was performed
960 using one-way ANOVA and Tukey HSD post hoc test: none were significantly different at
961 $p < 0.05$. A representative western blot from each group of experiments is shown.
962 C,D: Histone 3 lysine acetylation ('H3Kac', (C)) and histone 4 lysine acetylation ('H4Kac', (D))
963 were measured in *P. knowlesi* parasites grown in different concentrations of L-lactate for
964 8h, as in figure 1; data represented as in (A,B).
965 E,F: Histone 3 lysine acetylation ('H3Kac', (E)) and histone 4 lysine acetylation ('H4Kac', (F))
966 were measured in *P. falciparum* parasites grown either in 25mM L-lactate, or in control
967 media without added lactate, for 12h, then washed into fresh media, as in figure 2.
968 Samples were taken for western blotting at intervals from 0 to 24h. Stage of the parasite
969 culture is shown on the x-axis: ET, early trophozoite; MT, mid trophozoite; LT, late
970 trophozoite; S, schizont; R, ring. Graph shows data (mean and range) from two
971 independent timecourse experiments, each quantified as fold-changes from time-0 in the
972 signal of Kac versus total-H4, with one representative western blot shown.
973 G,H: Histone 3 lysine acetylation ('H3Kac', (G)) and histone 4 lysine acetylation ('H4Kac', (H))
974 were measured in *P. knowlesi* parasites grown either in 25mM L-lactate, or in control
975 media without added lactate, for 8h, then washed into fresh media, as in figure 2.
976 Samples were taken for western blotting at intervals from 0 to 20h. Stage of the parasite
977 culture is shown on the x-axis; data represented as in (E,F).
978
979 4. Histone lactylation is distributed throughout the nucleus
980 Confocal microscopy images showing the location of lactyl PTMs and of HP1 in *P.*
981 *falciparum* 3D7 HP1_HA. Lactyl-lysine, red; HP1_HA, green; DAPI, blue. KLa (A) and
982 H4K12La (B) distributions are mostly nuclear, and do not colocalise specifically with HA-
983 tagged HP1. T, trophozoite stage; S, schizont stage. Scale bar (2 µm) applies to all
984 images.
985
986 5. Histone lactylation occurs on multiple histone lysine residues in two *Plasmodium* species
987 A: Sequence alignments of histone tails in *P. falciparum* and *P. knowlesi*, showing in red all
988 KLa sites detected by mass spectrometry (either in trophozoite or mixed-stage cultures,

989 +/- 25mM lactate). Numbers in pink flanking the peptide sequences are residue
990 numbers of the N- and C-termini of the peptides. The tail of histone H2A is not shown
991 because no KLa was detected on this histone.
992 B: Pie charts representing the distribution of KLa sites from (A), and heatmaps representing
993 normalized intensities of KLa-containing peptides (Z-score transformed). Hierarchical
994 clustering was used to partition the KLa sites into 3 clusters with euclidean distance and
995 ward.D clustering algorithm. The time windows for trophozoite cultures of *P. falciparum*
996 and *P. knowlesi* were 24-26 and 12-14 hpi, respectively.
997
998 6. <u>Changes in PTMs on both histones and non-histone proteins are induced by exposure to</u>
999 <u>high lactate</u>
1000 Volcano plots representing (A) histones with differential lysine lactylation (KLa) and
1001 acetylation (Kac), in the top panels, and differential tri- or di-methylation (Kme3, Kme2)
1002 in the lower panels; (B) non-histone proteins with differential lysine lactylation (KLa).
1003 In all plots, data are from trophozoite cultures of *P. falciparum* or *P. knowlesi*, +/- 25mM
1004 lactate treatment. X-axes represent $\log_2$ fold changes (FC) calculated from normalized
1005 intensities, and y-axes represent *P*-values. Colored dots represent PTMs that changed
1006 significantly after lactate exposure, based on their significance threshold indicated by *P*-
1007 value. (Grey dots represent those that did not change significantly.) Symbols for histones
1008 and non-histones are hatched and filled circles, respectively. Horizontal and vertical lines
1009 represent *P*-value and $\log_2$FC significance thresholds.
1010 In (B), gene name abbreviations in *P. falciparum*, on the left: RNA MT, RNA
1011 methyltransferase; Histone AT, Histone acetyltransferase; LSD1, lysine specific histone
1012 demethylase; TsaD, TSaD-domain-containing protein; RBP25, RNA binding protein 25; RP
1013 L46, Ribosomal protein L46; G3P, glyceradehyde-3-phosphate dehydrogenase.
1014 In *P. knowlesi* on the right: snRNP PRP4, small nuclear ribonucleoprotein; HDAC SAP18,
1015 histone deacetylase subunit SAP18; Ser/Thr PK, serine/threonine protein kinase, CCR4-
1016 NOT, CCR4-NOT complex; PRP5 helicase, Pre-mRNA-processing ATP-dependent RNA
1017 helicase; SET2, SET2 histone methyltransferase.
1018
1019 7. <u>Gene ontology (GO) enrichment analysis of biological processes and cellular components</u>
1020 <u>enriched in PTMs after lactate exposure</u>
1021 Charts represent the top 5 GO terms (biological processes (A), cellular components (B))
1022 with the highest P-value for each PTM. Triangles mark the GO terms associated with
1023 proteins whose PTMs were upregulated; circles mark those down-regulated. Shapes are
1024 color-coded based on the magnitude of the fold change. The size of the shape,
1025 represented by Z-score, indicates the magnitude of the likelihood that the term is up- or
1026 down-regulated. *P.f* and *P.k* represent *P. falciparum* (all data on the left of the vertical
1027 dashed line) and *P. knowlesi* (right of dashed line). For simplicity, K(me3) and K(me2) are
1028 both presented as K(me). 'KLa' refers to all KLa sites detected; KLa.Sig refers to lactylated
1029 proteins that changed significantly upon lactate exposure in trophozoites.

1030

1031 8. <u>In rodent malaria parasites *in vivo,* transcriptomic profiles and lactylation of</u>
1032 <u>representative genes both vary with levels of host lactataemia</u>

1033 A: Volcano plots representing differentially expressed genes detected in late versus early
1034 infections of *P. yoelii* 17XL (top) and *P. berghei* ANKA (bottom). X-axes represent $\log_2$ fold
1035 changes (FC) calculated from normalized CPM values; y-axes represent *P*-values.
1036 Coloured dots represent DE genes, based on their significance threshold indicated by
1037 adjusted *P*-value (FDR) (purple dots represent those below any significance threshold).
1038 Horizontal and vertical dashed lines represent *P*-value and $\log_2$FC significance thresholds.
1039 Gene name abbrevations in *P. yoelli*: SP15, transcription elongation factor SPT5; TIFII,
1040 eukaryotic translation initiation factor 3 subunit L; HSP20, HSP20-like chaperone; nPrx,
1041 peroxiredoxin; PFK11, ATP-dependent 6-phosphofructokinase; H2B, histone H2B; H4,
1042 histone H4; SOD2, superoxide dismutase [Fe]; GEST, gamete egress and sporozoite
1043 traversal protein; L-LDH, L-lactate dehydrogenase; LDH, lactate dehydrogenase; FD3,
1044 female development protein FD3; H2B.Z, Histone H2B variant; MDV1, male development
1045 protein 1; FD1, female development protein 1.
1046 Gene name abbrevations in *P. berghei*: ApiAP2, AP2 domain transcription factor;
1047 GSK3beta, glycogen synthase kinase-3 beta; GNAT, N-acetyltransferase in GNAT family;
1048 MCM2/5/9, DNA replication licensing factor MCM2/5/9; RECQ1, ATP-dependent DNA
1049 helicase RecQ1; SET7, histone-lysine N-methyltransferase SET7; G3PDH, glycerol-3-
1050 phosphate dehydrogenase; RIP, PIR protein; Sir2A, histone deacetylase Sir2A; CAF1B,
1051 chromatin assembly factor 1 subunit B.

1052 B: Heatmaps representing late and early transcriptional profiles in $\log_2$CPM (Z-score
1053 transformed) for DE genes (502 in *P. yoelii*, 1521 in *P. berghei*). Hierarchical clustering
1054 was performed to cluster genes expression profiles with euclidean distance and ward.D
1055 clustering algorithm.

1056 C: Boxplot showing KLa enrichment detected via ChIP in the CDS of five *P. yoelii* genes
1057 whose expression significantly changed in response to hyperlactataemia (sig. regulated),
1058 and nine genes whose expression did not (non sig. regulated). Y-axis represents the
1059 percentage of chromatin input recovery (% IPed) for each ChIPed region. One biological
1060 replicate for each of three mice (i.e. three lactate conditions). Dots represent individual
1061 genes, horizontal line represents median, box represents interquartile range, whiskers
1062 represent variability outside the interquartile range (quartile -/+ 1.5 * IQR). Multiple
1063 comparison of means was performed using ANOVA and Tukey HSD post hoc tests at *p-*
1064 *value* < 0.05 for between-group comparison. Left boxplot (ANOVA, F = 0.788 ; d.fsum = 2;
1065 p-value = 0.466), right boxplot (ANOVA, F = 23.73; d.fsum = 2; p-value = 6.76e-05). *** p-
1066 value ≤ 0.001; ** p-value ≤ 0.01; *p-value ≤ 0.05; ns, not significant.

1067 D: Biological process gene ontology (GO) enrichment analysis of DE genes in *P. berghei* and
1068 *P. yoelii.* Plots show the top 15 GO terms with the highest *P*-values. The outer circle
1069 displays scatterplots of the expression levels ($\log_2$FC) for the genes (dots) in each GO
1070 term, whereas the inner circle is a bar plot where the height of the bar indicates the

significance of the term (−log10 *P*-value). The colour corresponds to the Z-score, which indicates whether the term is likely to be decreased (negative value) or increased (positive value).

Figure 1

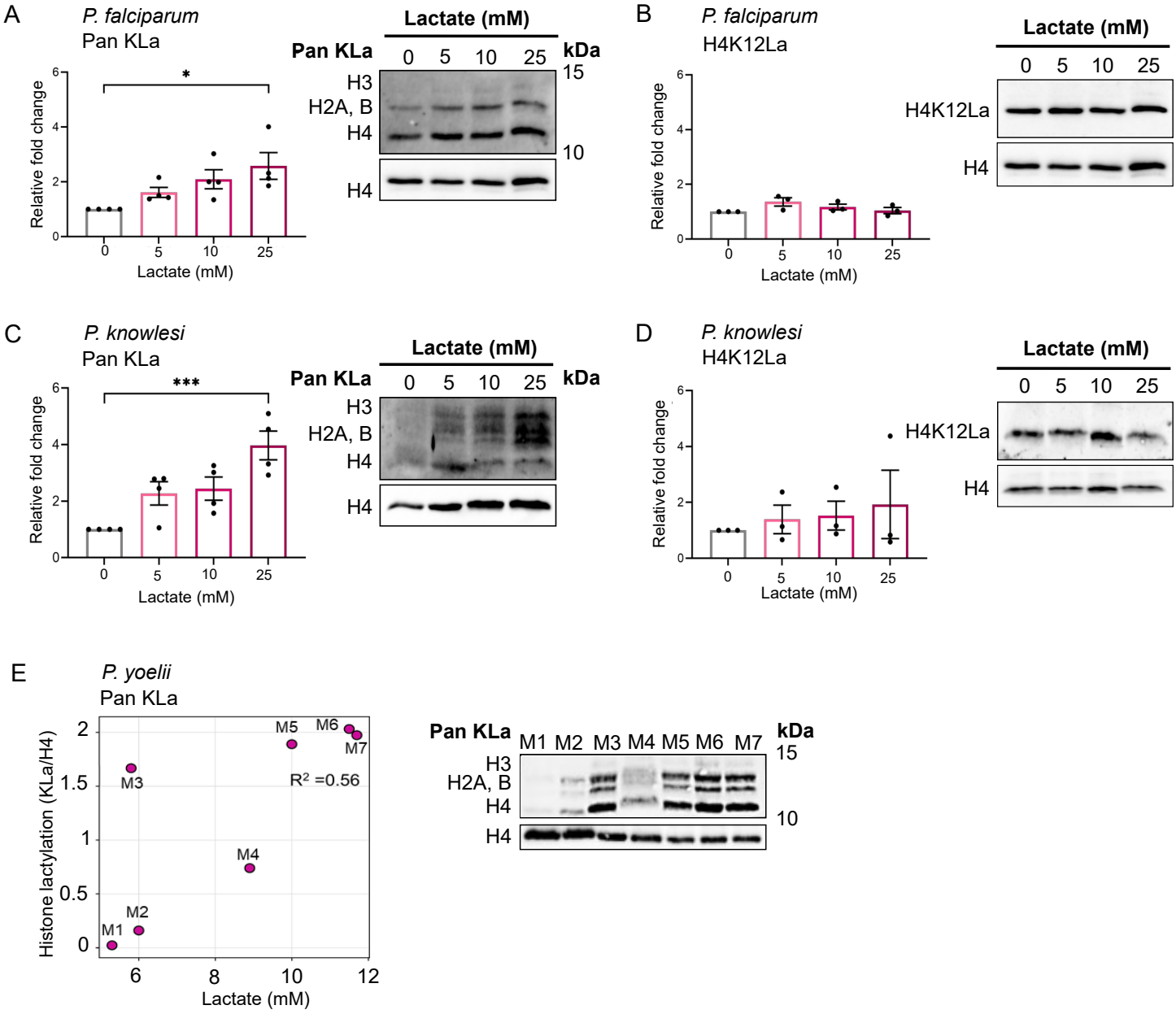
A
P. falciparum
Pan KLa
Relative fold change
Lactate (mM)
Pan KLa
Lactate (mM)
0 5 10 25
kDa
15
10
H3
H2A, B
H4
H4
B
P. falciparum
H4K12La
H4K12La
H4
C
P. knowlesi
Pan KLa
D
P. knowlesi
H4K12La
E
P. yoelii
Pan KLa
Histone lactylation (KLa/H4)
M1 M2 M3 M4 M5 M6 M7
R² =0.56

Figure 2

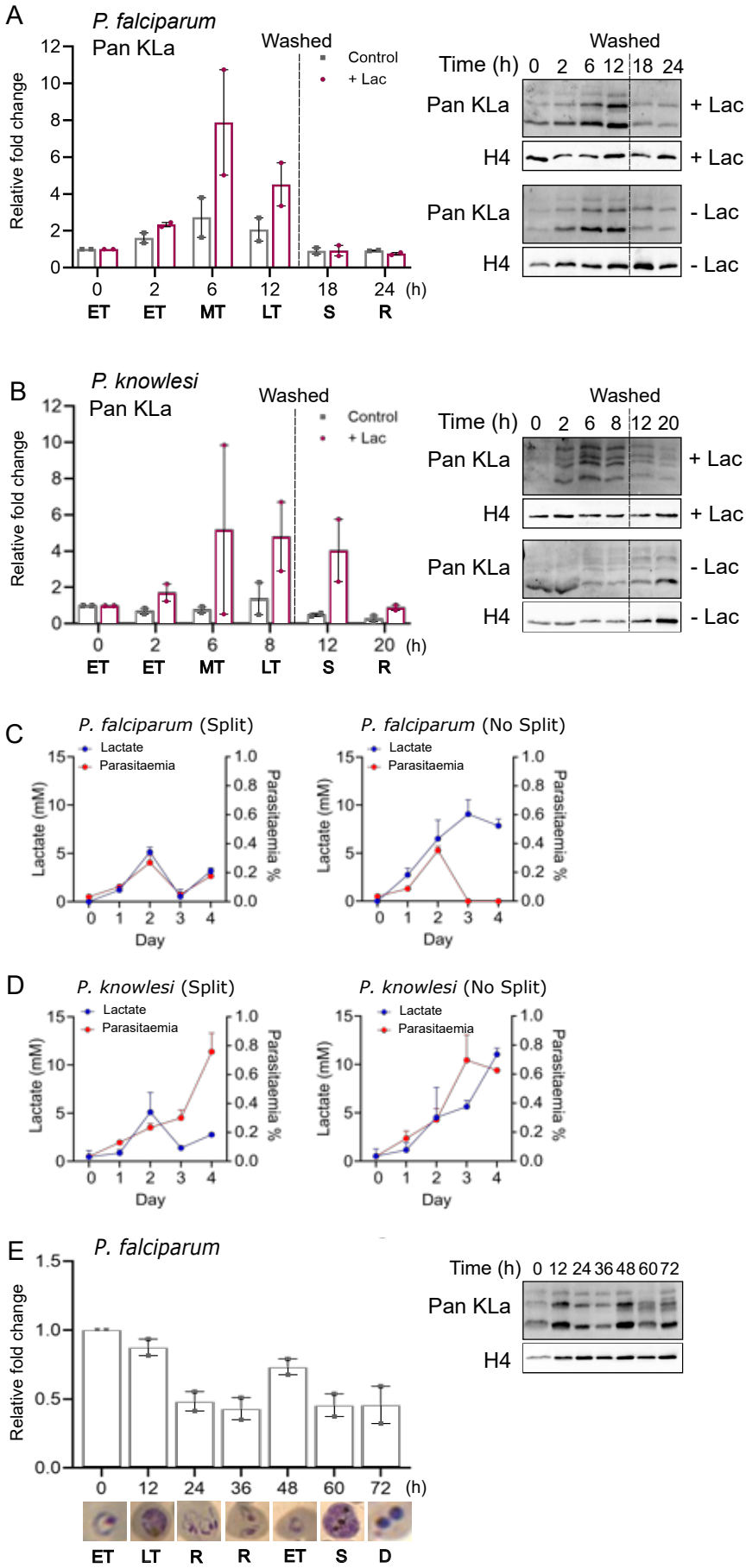
A
P. falciparum
Pan KLa
Washed
Control
+ Lac
Relative fold change
0 2 6 12 18 24 (h)
ET ET MT LT S R
Time (h) 0 2 6 12 18 24
Pan KLa
H4
+ Lac
- Lac
B
P. knowlesi
Pan KLa
Washed
Control
+ Lac
Relative fold change
0 2 6 8 12 20 (h)
ET ET MT LT S R
Time (h) 0 2 6 8 12 20
C
P. falciparum (Split)
P. falciparum (No Split)
Lactate
Parasitaemia
Lactate (mM)
Parasitaemia %
Day
D
P. knowlesi (Split)
P. knowlesi (No Split)
E
P. falciparum
Relative fold change
0 12 24 36 48 60 72 (h)
ET LT R R ET S D
Time (h) 0 12 24 36 48 60 72

Figure 3

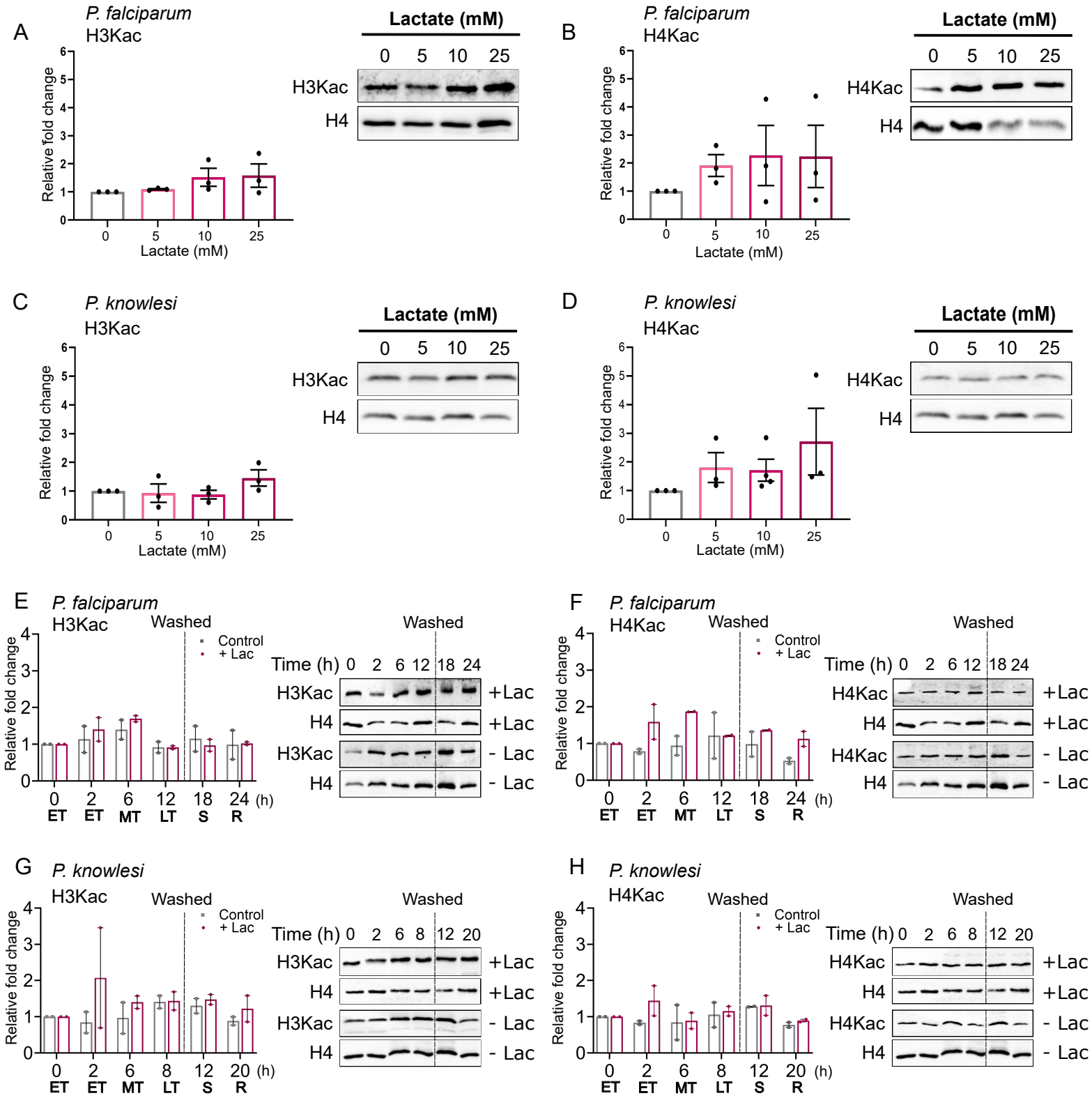
A
P. falciparum
H3Kac
Relative fold change
Lactate (mM)
0 5 10 25
H3Kac
H4
B
P. falciparum
H4Kac
C
P. knowlesi
H3Kac
D
P. knowlesi
H4Kac
E
P. falciparum
H3Kac
Washed
Control
+ Lac
Time (h) 0 2 6 12 18 24
+Lac
- Lac
0 2 6 12 18 24 (h)
ET ET MT LT S R
F
P. falciparum
H4Kac
G
P. knowlesi
H3Kac
Time (h) 0 2 6 8 12 20
0 2 6 8 12 20 (h)
ET ET MT LT S R
H
P. knowlesi
H4Kac

Figure 4

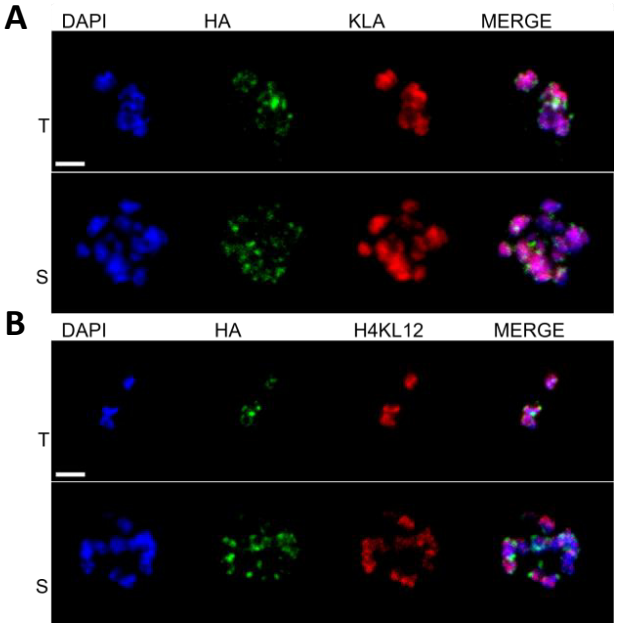

Figure 5

A

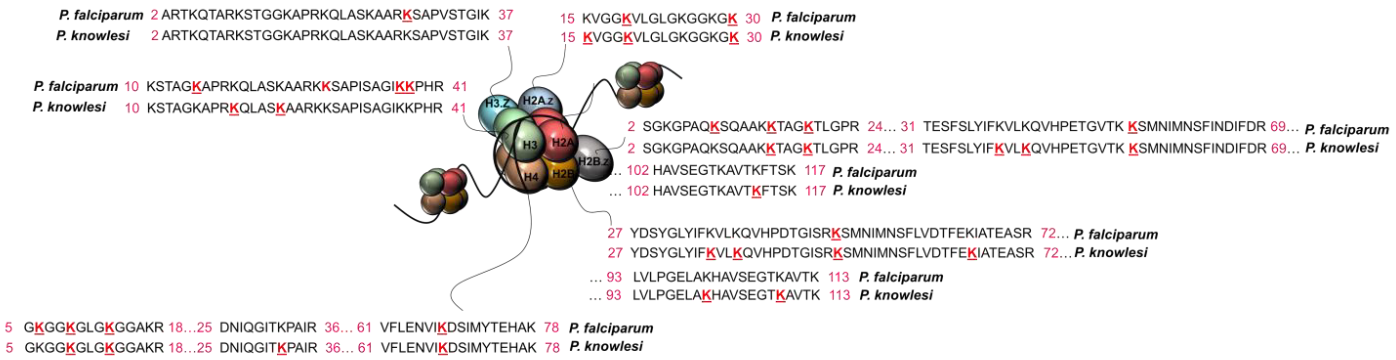
P. falciparum 2 ARTKQTARKSTGGKAPRKQLASKAARKSAPVSTGIK 37
P. knowlesi 2 ARTKQTARKSTGGKAPRKQLASKAARKSAPVSTGIK 37
P. falciparum 10 KSTAGKAPRKQLASKAARKKSAPISAGIKKPHR 41
P. knowlesi 10 KSTAGKAPRKQLASKAARKKSAPISAGIKKPHR 41
15 KVGGKVLGLGKGGKGK 30 P. falciparum
15 KVGGKVLGLGKGGKGK 30 P. knowlesi
H3.Z
H2A.z
H3
H2A
H4
H2B.z
H2B
2 SGKGPAQKSQAAKKTAGKTLGPR 24... 31 TESFSLYIFKVLKQVHPETGVTK KSMNIMNSFINDIFDR 69... P. falciparum
2 SGKGPAQKSQAAKKTAGKTLGPR 24... 31 TESFSLYIFKVLKQVHPETGVTK KSMNIMNSFINDIFDR 69... P. knowlesi
... 102 HAVSEGTKAVTKFTSK 117 P. falciparum
... 102 HAVSEGTKAVTKFTSK 117 P. knowlesi
27 YDSYGLYIFKVLKQVHPDTGISRKSMNIMNSFLVDTFEKIATEASR 72... P. falciparum
27 YDSYGLYIFKVLKQVHPDTGISRKSMNIMNSFLVDTFEKIATEASR 72... P. knowlesi
... 93 LVLPGELAKHAVSEGTKAVTK 113 P. falciparum
... 93 LVLPGELAKHAVSEGTKAVTK 113 P. knowlesi
5 GKGGKGLGKGGAKR 18...25 DNIQGITKPAIR 36... 61 VFLENVIKDSIMYTEHAK 78 P. falciparum
5 GKGGKGLGKGGAKR 18...25 DNIQGITKPAIR 36... 61 VFLENVIKDSIMYTEHAK 78 P. knowlesi

B

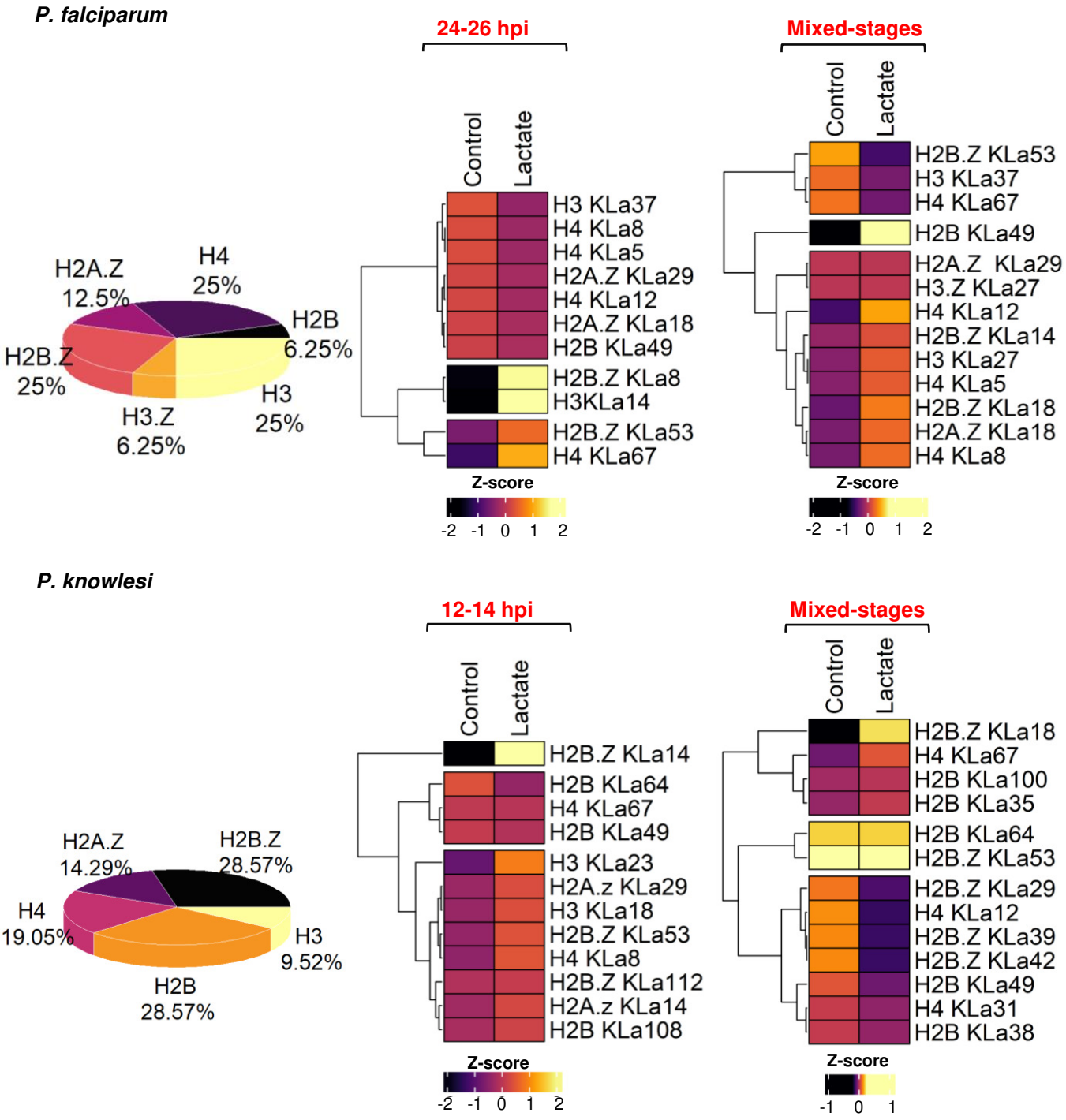
P. falciparum
24-26 hpi
Mixed-stages
Control
Lactate
H2A.Z 12.5%
H4 25%
H2B 6.25%
H2B.Z 25%
H3 25%
H3.Z 6.25%
H3 KLa37
H4 KLa8
H4 KLa5
H2A.Z KLa29
H4 KLa12
H2A.Z KLa18
H2B KLa49
H2B.Z KLa8
H3KLa14
H2B.Z KLa53
H4 KLa67
Z-score
-2 -1 0 1 2
H2B.Z KLa53
H3 KLa37
H4 KLa67
H2B KLa49
H2A.Z KLa29
H3.Z KLa27
H4 KLa12
H2B.Z KLa14
H3 KLa27
H4 KLa5
H2B.Z KLa18
H2A.Z KLa18
H4 KLa8
Z-score
-2 -1 0 1 2
P. knowlesi
12-14 hpi
Mixed-stages
Control
Lactate
H2A.Z 14.29%
H2B.Z 28.57%
H4 19.05%
H3 9.52%
H2B 28.57%
H2B.Z KLa14
H2B KLa64
H4 KLa67
H2B KLa49
H3 KLa23
H2A.z KLa29
H3 KLa18
H2B.Z KLa53
H4 KLa8
H2B.Z KLa112
H2A.z KLa14
H2B KLa108
Z-score
-2 -1 0 1 2
H2B.Z KLa18
H4 KLa67
H2B KLa100
H2B KLa35
H2B KLa64
H2B.Z KLa53
H2B.Z KLa29
H4 KLa12
H2B.Z KLa39
H2B.Z KLa42
H2B KLa49
H4 KLa31
H2B KLa38
Z-score
-1 0 1

Figure 6

A

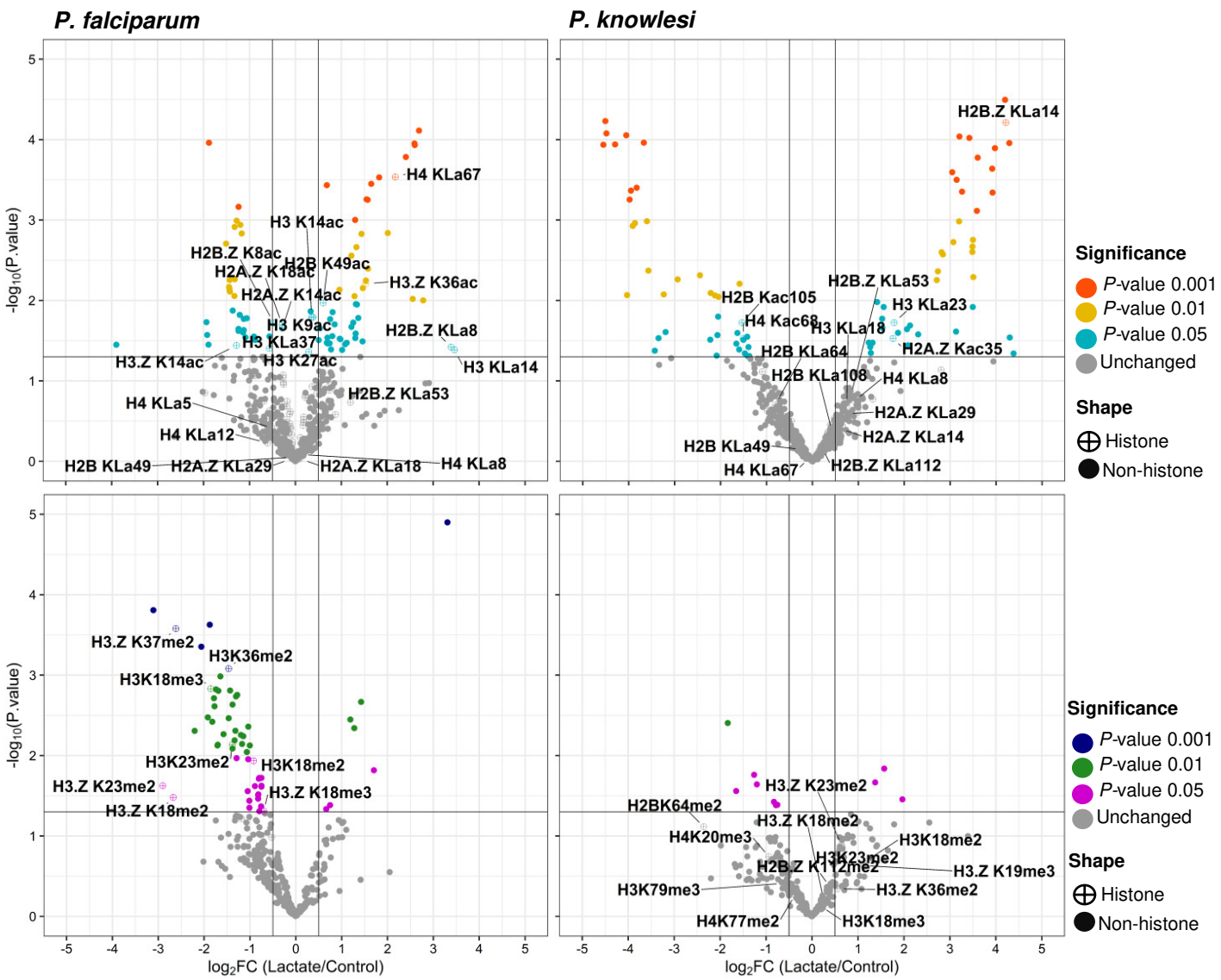
P. falciparum
P. knowlesi
-log10(P.value)
log2FC (Lactate/Control)
H4 KLa67
H3 K14ac
H2B.Z K8ac
H2A.Z K18ac
H2B K49ac
H3.Z K36ac
H2A.Z K14ac
H3 K9ac
H3 KLa37
H2B.Z KLa8
H3.Z K14ac
H3 K27ac
H3 KLa14
H2B.Z KLa53
H4 KLa5
H4 KLa12
H2B KLa49
H2A.Z KLa29
H2A.Z KLa18
H4 KLa8
H2B.Z KLa14
H2B.Z KLa53
H2B Kac105
H3 KLa23
H4 Kac68
H3 KLa18
H2A.Z Kac35
H2B KLa64
H2B KLa108
H4 KLa8
H2A.Z KLa29
H2A.Z KLa14
H2B KLa49
H4 KLa67
H2B.Z KLa112
H3.Z K37me2
H3K36me2
H3K18me3
H3K23me2
H3K18me2
H3.Z K23me2
H3.Z K18me3
H3.Z K18me2
H3.Z K23me2
H2BK64me2
H3.Z K18me2
H4K20me3
H3K18me2
H3K23me2
H2B.Z K112me2
H3.Z K19me3
H3K79me3
H3.Z K36me2
H4K77me2
H3K18me3
Significance
P-value 0.001
P-value 0.01
P-value 0.05
Unchanged
Shape
Histone
Non-histone

B

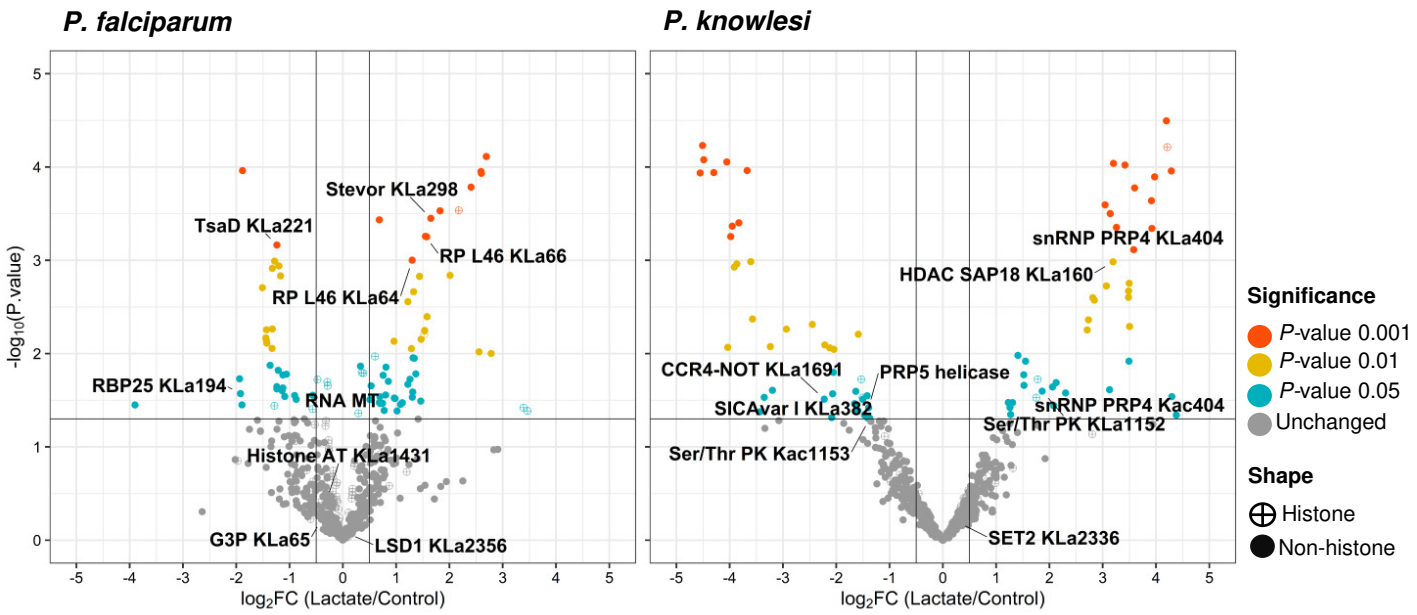
P. falciparum
P. knowlesi
-log10(P.value)
log2FC (Lactate/Control)
Stevor KLa298
TsaD KLa221
RP L46 KLa66
RP L46 KLa64
RBP25 KLa194
RNA MT
Histone AT KLa1431
G3P KLa65
LSD1 KLa2356
snRNP PRP4 KLa404
HDAC SAP18 KLa160
CCR4-NOT KLa1691
PRP5 helicase
SICAvar I KLa382
snRNP PRP4 Kac404
Ser/Thr PK KLa1152
Ser/Thr PK Kac1153
SET2 KLa2336
Significance
P-value 0.001
P-value 0.01
P-value 0.05
Unchanged
Shape
Histone
Non-histone

Figure 7

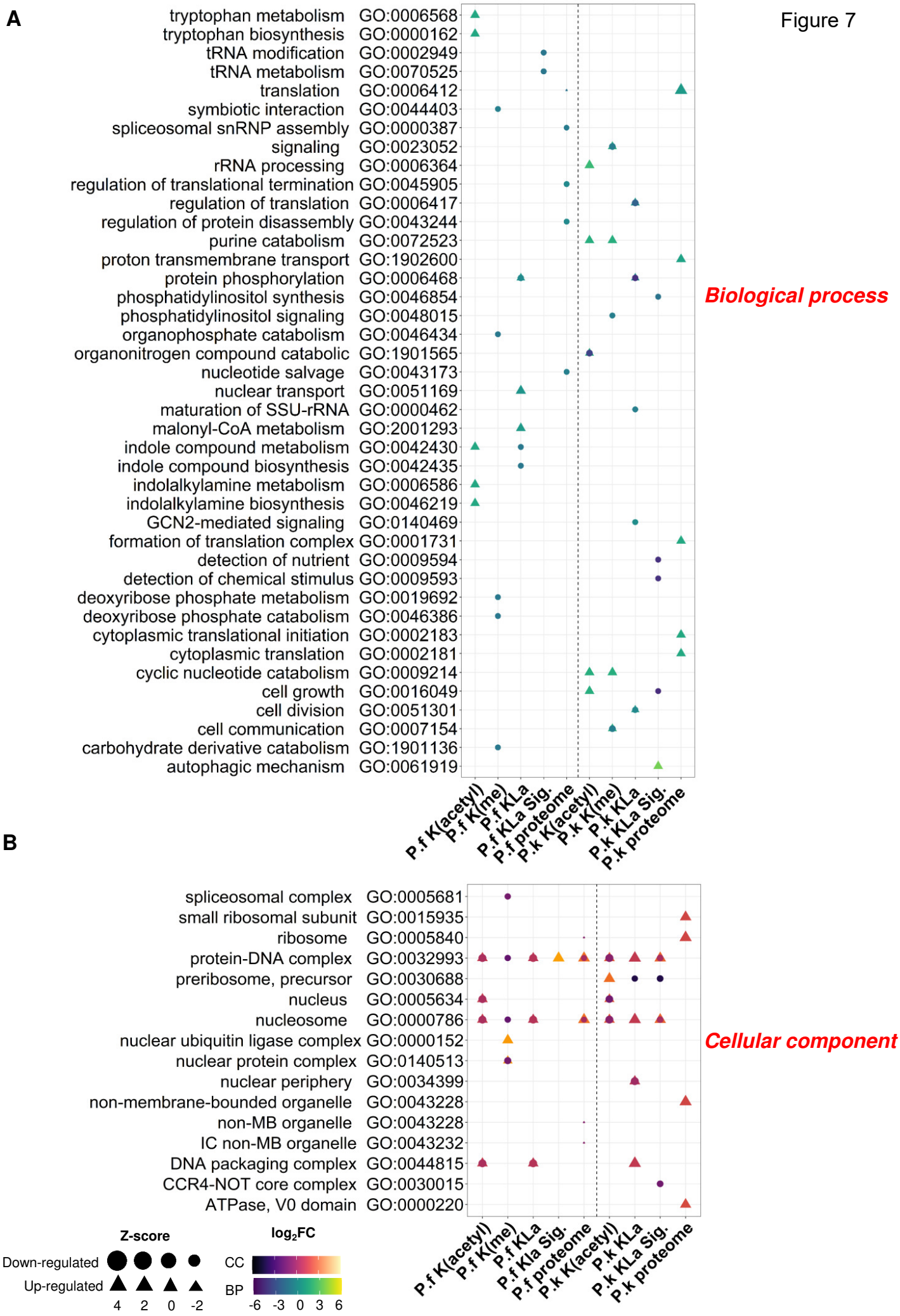
A
tryptophan metabolism GO:0006568
tryptophan biosynthesis GO:0000162
tRNA modification GO:0002949
tRNA metabolism GO:0070525
translation GO:0006412
symbiotic interaction GO:0044403
spliceosomal snRNP assembly GO:0000387
signaling GO:0023052
rRNA processing GO:0006364
regulation of translational termination GO:0045905
regulation of translation GO:0006417
regulation of protein disassembly GO:0043244
purine catabolism GO:0072523
proton transmembrane transport GO:1902600
protein phosphorylation GO:0006468
phosphatidylinositol synthesis GO:0046854
phosphatidylinositol signaling GO:0048015
organophosphate catabolism GO:0046434
organonitrogen compound catabolic GO:1901565
nucleotide salvage GO:0043173
nuclear transport GO:0051169
maturation of SSU-rRNA GO:0000462
malonyl-CoA metabolism GO:2001293
indole compound metabolism GO:0042430
indole compound biosynthesis GO:0042435
indolalkylamine metabolism GO:0006586
indolalkylamine biosynthesis GO:0046219
GCN2-mediated signaling GO:0140469
formation of translation complex GO:0001731
detection of nutrient GO:0009594
detection of chemical stimulus GO:0009593
deoxyribose phosphate metabolism GO:0019692
deoxyribose phosphate catabolism GO:0046386
cytoplasmic translational initiation GO:0002183
cytoplasmic translation GO:0002181
cyclic nucleotide catabolism GO:0009214
cell growth GO:0016049
cell division GO:0051301
cell communication GO:0007154
carbohydrate derivative catabolism GO:1901136
autophagic mechanism GO:0061919
P.f K(acetyl)
P.f K(me)
P.f KLa
P.f KLa Sig.
P.f proteome
P.k K(acetyl)
P.k K(me)
P.k KLa
P.k KLa Sig.
P.k proteome
Biological process
B
spliceosomal complex GO:0005681
small ribosomal subunit GO:0015935
ribosome GO:0005840
protein-DNA complex GO:0032993
preribosome, precursor GO:0030688
nucleus GO:0005634
nucleosome GO:0000786
nuclear ubiquitin ligase complex GO:0000152
nuclear protein complex GO:0140513
nuclear periphery GO:0034399
non-membrane-bounded organelle GO:0043228
non-MB organelle GO:0043228
IC non-MB organelle GO:0043232
DNA packaging complex GO:0044815
CCR4-NOT core complex GO:0030015
ATPase, V0 domain GO:0000220
P.f K(acetyl)
P.f K(me)
P.f KLa
P.f KLa Sig.
P.f proteome
P.k K(acetyl)
P.k KLa
P.k KLa Sig.
P.k proteome
Cellular component
Z-score
Down-regulated
Up-regulated
4 2 0 -2
log2FC
CC
BP
-6 -3 0 3 6

Figure 8

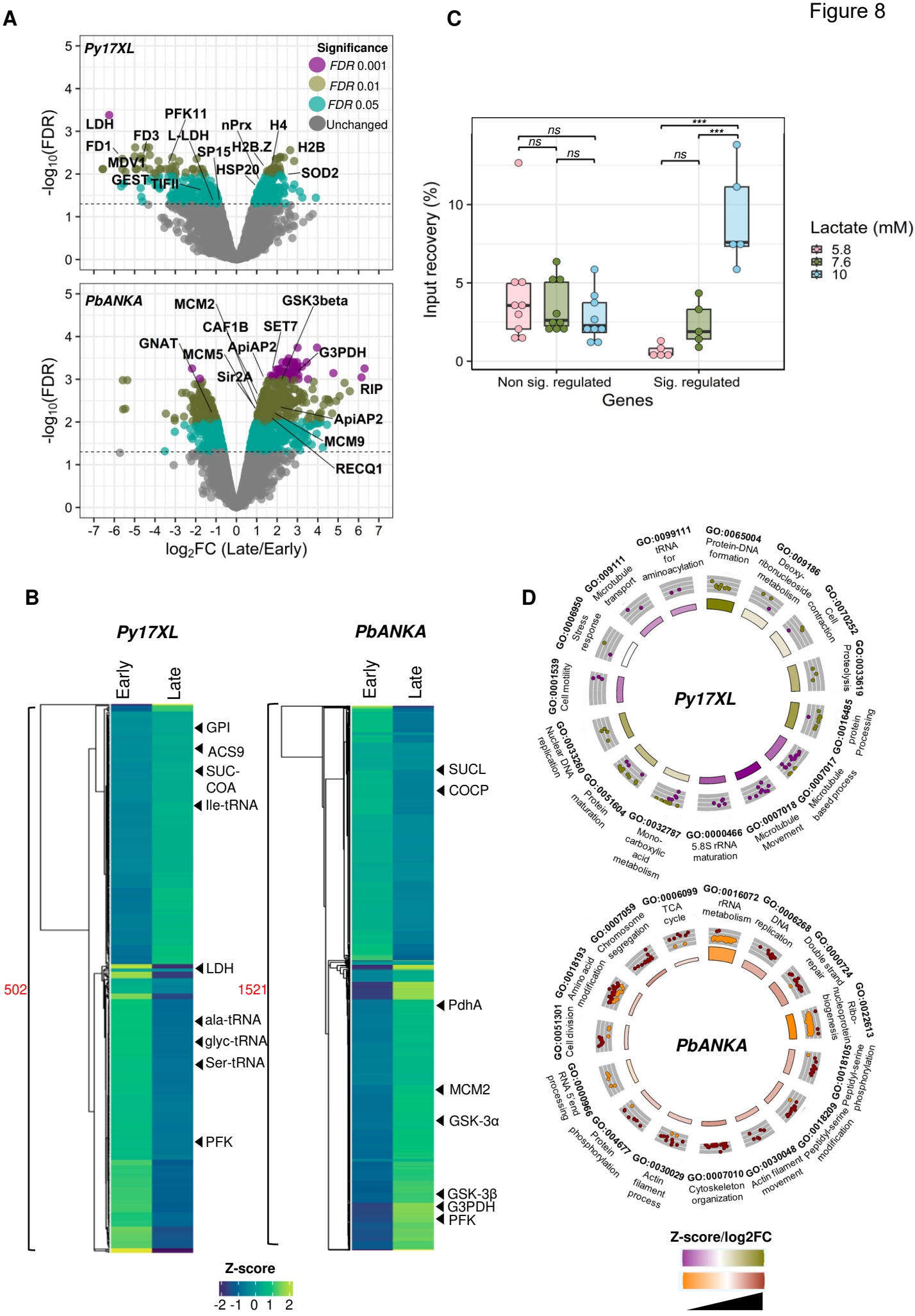
A
Py17XL
Significance
FDR 0.001
FDR 0.01
FDR 0.05
Unchanged
LDH
FD1
FD3
MDV1
GEST
TIFII
PFK11
L-LDH
SP15
nPrx
H2B.Z
HSP20
H4
H2B
SOD2
-log10(FDR)
PbANKA
MCM2
GSK3beta
CAF1B
SET7
GNAT
MCM5
ApiAP2
G3PDH
Sir2A
RIP
ApiAP2
MCM9
RECQ1
log2FC (Late/Early)
C
Input recovery (%)
ns
***
Non sig. regulated
Sig. regulated
Genes
Lactate (mM)
5.8
7.6
10
B
Py17XL
PbANKA
Early
Late
GPI
ACS9
SUC-COA
Ile-tRNA
LDH
ala-tRNA
glyc-tRNA
Ser-tRNA
PFK
502
1521
SUCL
COCP
PdhA
MCM2
GSK-3α
GSK-3β
G3PDH
PFK
Z-score
D
Py17XL
GO:0065004 Protein-DNA formation
GO:0099111 tRNA for aminoacylation
GO:0009186 Deoxy-ribonucleoside metabolism
GO:0070252 Cell contraction
GO:0003619 Proteolysis
GO:0016485 protein Processing
GO:0007017 Microtubule based process
GO:0007018 Microtubule Movement
GO:0000466 5.8S rRNA maturation
GO:0032787 Mono-carboxylic acid metabolism
GO:0051604 Protein maturation
GO:0033260 Nuclear DNA replication
GO:0001539 Cell motility
GO:0006950 Stress response
GO:0009111 Microtubule transport
PbANKA
GO:0016072 rRNA metabolism
GO:0006099 TCA cycle
GO:0006268 DNA replication
GO:0000724 Double-strand repair
GO:0022613 Ribo-nucleoprotein biogenesis
GO:0018105 Peptidyl-serine phosphorylation
GO:0018209 Peptidyl-serine modification
GO:0030048 Actin filament movement
GO:0007010 Cytoskeleton organization
GO:0030029 Actin filament process
GO:0004677 Protein phosphorylation
GO:0000966 RNA 5'end processing
GO:0051301 Cell division
GO:0018193 Amino acid modification
GO:0007059 Chromosome segregation
Z-score/log2FC